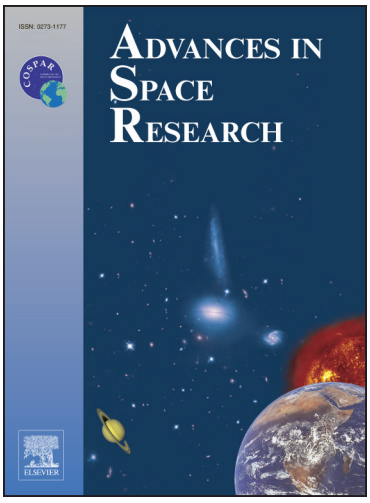

Traverses for the ISECG-GER Design Reference Mission for Humans on the Lunar Surface

Elyse J. Allender, Csilla Orgel, Natasha V. Almeida, John Cook, Jessica J. Ende, Oscar Kamps, Sara Mazrouei, Thomas J. Slezak, Assi-Johanna Soini, David A. Kring

PII: S0273-1177(18)30660-4
DOI: https://doi.org/10.1016/j.asr.2018.08.032
Reference: JASR 13897

To appear in: *Advances in Space Research*

Received Date: 12 April 2018
Accepted Date: 21 August 2018

Please cite this article as: Allender, E.J., Orgel, C., Almeida, N.V., Cook, J., Ende, J.J., Kamps, O., Mazrouei, S., Slezak, T.J., Soini, A-J., Kring, D.A., Traverses for the ISECG-GER Design Reference Mission for Humans on the Lunar Surface, *Advances in Space Research* (2018), doi: https://doi.org/10.1016/j.asr.2018.08.032

Traverses for the ISECG-GER Design Reference Mission for Humans on the Lunar Surface

Elyse J. Allender[a,*], Csilla Orgel[b], Natasha V. Almeida[c], John Cook[d], Jessica J. Ende[e], Oscar Kamps[f], Sara Mazrouei[g], Thomas J. Slezak[h], Assi-Johanna Soini[i], David A. Kring[j]

[a]*School of Earth and Environmental Sciences, University of St Andrews, St Andrews, UK*
[b]*Institute of Geological Sciences, Planetary Sciences and Remote Sensing, Freie Universität Berlin, Germany*
[c]*Planetary Materials Group, Department of Earth Sciences, Natural History Museum, London, UK*
[d]*University of Houston, USA*
[e]*Department of Earth and Planetary Sciences, University of Tennessee Knoxville, USA*
[f]*ITC Faculty of Geo-Information Science and Earth Observation, University of Twente, Enschede, The Netherlands*
[g]*Department of Earth Sciences, University of Toronto, Toronto, Canada*
[h]*Department of Geological Sciences, Brigham Young University, Provo, USA*
[i]*Department of Physics, University of Helsinki, Helsinki, Finland*
[j]*Center for Lunar Science and Exploration, Lunar and Planetary Institute, Houston, USA*

*Corresponding author.
Email address: ea63@st-andrews.ac.uk (Elyse J. Allender)

Abstract

This study explores the Design Reference Mission (DRM) architecture developed by Hufenbach et al. (2015) as a prelude to the release of the 2018 Global Exploration Roadmap (GER) developed by the International Space Exploration Coordination Group (ISECG). The focus of this study is the exploration of the south polar region of the Moon, a region that has not been visited by any human missions, yet exhibits a multitude of scientifically important locations – the investigation of which will address long standing questions in lunar research. This DRM architecture involves five landing sites (Malapert massif, South Pole /Shackleton crater, Schrödinger basin, Antoniadi crater, and the South Pole-Aitken basin center), to be visited in sequential years by crew, beginning in 2028. Two Lunar Electric Rovers (LER) are proposed to be tele-robotically operated between sites to rendez-vous with crew at the time of the next landing. With engineering parameters in mind we explore the feasibility of tele-robotic operation of these LERs between lunar landing sites, and identify potential high interest sampling locations en-route. Additionally, in-depth sample collection and return traverses are identified for each individual landing site across key geologic terrains that also detail crew Extra-Vehicular Activity (EVA). Exploration at and between landing sites is designed to address a suite of National Research Council (National Research Council, 2007) scientific concepts.

Keywords: Moon, Lunar exploration, Design Reference Mission, Sample return, South Pole-Aitken Basin, Landing sites

1. Introduction

As the international community continues to move forward with its vision for Solar System exploration, it is important to articulate a framework for inter-agency discussion and collaboration so that vital scientific questions may be addressed, and the overall strategic vision enhanced. The Global Exploration Roadmap (GER) provides such a framework. Developed by the International Space Exploration Coordination Group (ISECG) and last updated in 2018, the GER communicates a vision for collaborative and coordinated exploration of the Solar System, beginning with the International Space Station (ISS), continuing to the Moon and, eventually, leading to human missions on Mars (International Space Exploration Coordination Group, 2018).

Prior to the publication of the 2018 GER, envisaged updates to the 2013 version (International Space Exploration Coordination Group, 2013) were presented by Hufenbach et al. (2015), who summarized the status of Design Reference Missions (DRM) targeting the lunar vicinity and surface, and highlighted the value these missions have for advancing the implementation of the GER. Hufenbach et al. (2015) also identified several opportunities for international cooperation and outlined a set of mission themes. This study examines the third theme – Humans to the Lunar Surface – and, in particular, its second phase 'Human Lunar Surface Missions'.

The plan for Human Lunar Surface Missions is shaped by science, strategies for surface campaigns, and a Mars-forward perspective. The proposed missions focus on the south polar region and target five sites of diverse scientific interest: Malapert massif (85.99°S, 2.93°W), the South Pole/Shackleton crater (89.3°S, 130.0°W), Schrödinger basin (75.40°S, 138.77°E), Antoniadi crater (69.7°S, 172.0°W), and the South Pole-Aitken (SPA) basin center (60.0°S, 159.9°W). Here, we adjust the latitude and longitude of those sites slightly (Figure 1) in order to maximize scientific return within a 100 km Mars-forward exploration zone (Hufenbach et al., 2015). This exploration zone represents the maximum distance crewed rovers can travel from the landing site in order to return to a Lunar Orbital Platform-Gateway (LOP-G) within a 36 hr window in the event a mission abort is necessary (Whitley et al., 2017).

These sites are to be explored sequentially, beginning with Malapert massif. Before the first crew lands, two small pressurized rovers (SPRs), flight versions of the Lunar Electric Rover (LER), are delivered to the landing site.

Once a crew arrives, it uses the rovers to explore the local region. After crew return to a LOP-G with the ascent vehicle and deliver samples back to Earth using the Orion, the rovers are tele-robotically driven to the next landing site where they can be used by a second crew. At each landing site, a crew of four is deployed, with two assigned to each SPR.

Here, we design (i) traverses between the landing sites and (ii) traverses in the vicinity of each landing site. To guide the design of those traverses, we utilize the key science concepts and investigative goals summarized by the National Research Council (NRC) (National Research Council, 2007). We list the prioritized and ranked concepts below:

1. The bombardment history of the inner solar system is uniquely revealed on the Moon.
2. The structure and composition of the lunar interior provide fundamental information on the evolution of a differentiated planetary body.
3. Key planetary processes are manifested in the diversity of lunar crustal rocks.
4. Lunar volatiles increase our understanding of the composition state and distribution of volatiles in the lunar polar regions.
5. Lunar volcanism provides a window into the thermal and compositional evolution of the Moon.
6. The Moon is an accessible laboratory for studying the impact process on planetary scales.
7. The Moon is a natural laboratory for regolith processes and weathering on anhydrous airless bodies.
8. Processes involved with the atmosphere and dust environment of the Moon are accessible for scientific study while the environment remains in a pristine state.

Within these eight concepts are 35 specific science goals to be addressed. Concepts 1 to 7 and their associated goals provide the framework against which the feasibility of each location within this study is assessed. Concept 8 has been addressed by the Lunar Atmosphere Dust and Environment Explorer (LADEE) mission and is not considered further here as we focus on addressing lunar interior and surface goals.

These concepts and goals were previously evaluated in a global lunar landing site study (Kring and Durda, 2012) which objectively identified scientifically-rich landing site locations. One of the sites, the Schrödinger basin, was identified in that study to be the highest priority landing site on the lunar surface because of the broad range of science and exploration

objectives that could be addressed within that single location. Design reference missions, like those of Hufenbach et al. (2015) and Whitley et al. (2017), utilize a set of high-priority landing sites identified from Kring and Durda (2012) to realize exploration architecture set forth in the Global Exploration Roadmap (International Space Exploration Coordination Group, 2013, 2018).

This study 'closes the loop' in that we demonstrate how the design reference mission and engineering concepts of Hufenbach et al. (2015) can achieve the National Research Council (2007) goals and objectives using the mission architecture set forth in the Global Exploration Roadmap International Space Exploration Coordination Group (2013, 2018). We also utilize contributions from other landing site and traverse studies (Steenstra et al., 2016; Sruthi and Kumar, 2014; Kramer et al., 2013; Kring and Durda, 2012; Borst et al., 2012; Gibson and Jolliff, 2011). Steenstra et al. (2016), in particular, utilizes architecture from ISECGs European Space Agency led Human-Enhanced Robotic Architecture and Capability for Lunar Exploration (HERACLES) mission concept (Landgraf et al., 2015), demonstrating the growing interest in human-robotic partnership for future exploration. Insights and implied trade studies (section 6) arising from this work will help to further international collaboration on human-assisted robotic missions. It should be noted that once a formal landing site selection process has been performed by the international community the assessments within this paper can (and will) be performed again on the finalized selection.

Our results will be presented as follows: section 2 provides a general overview of the geology of the SPA basin and each proposed human landing site, section 3 details concept of operations information such as mission architecture elements, SPR functionality, sample collection requirements, and communication requirements. Section 4 details traverses between landing sites, and at and around each site – taking parameters such as safe driving distances, trafficability, orbital communications coverage, and sample collection masses into account. Also, the ability to address NRC (2007) is assessed. In section 6 we present recommendations for future trade studies, and section 7 contains the study's findings.

2. SPA Geology and Landing Sites

The South Pole-Aitken (SPA) basin is the largest (Smith et al., 2010) and oldest recognized impact structure (Wilhelms, 1987; Hiesinger et al., 2012;

Orgel et al., 2018) in the Solar System with a diameter of 2500 km and a depth of approximately 13 km (Smith et al., 2010). Such a large basin-forming impact may have had significant thermal and geophysical effects both locally and globally. Based on Gravity Recovery and Interior Laboratory (GRAIL) data SPA basin exhibits a crustal thickness of <20 km with local variations less than 5 km at Apollo and Poincaré basins (Wieczorek et al., 2013). Because of the large extent of the SPA basin forming impact surface components may represent some of the deepest lunar materials, such as lower crust and upper mantle, which could be available to study (Cintala and Grieve, 1998; Vaughan and Head, 2014). Significant olivine exposures have not yet been detected within the SPA interior, only localized exposures of olivine in central peak/peak ring structures have been observed in Schrödinger basin and Zeeman crater (Kramer et al., 2013; Yamamoto et al., 2012).

Generally, SPA materials show enrichment in mafic minerals (pyroxenes) relative to the feldspathic highlands (Lawrence et al., 2002; Pieters et al., 2001; Moriarty and Pieters, 2018). There is a zoning in the distribution of low-Ca pyroxenes (Mg-rich pyroxenes) across the basin (Pieters et al., 2001; Nakamura et al., 2009) and high-Ca pyroxenes in a 700 km region in the SPA basin interior, distinct from both mare basalts and Mg-pyroxenes (Moriarty and Pieters, 2016; Ohtake et al., 2014). Additionally, the SPA interior exhibits a distinctive high-FeO chemical signature (Lucey et al., 1998; Jolliff et al., 2000; Gibson and Jolliff, 2011; Ivanov et al., In Press) called the SPA Compositional Anomaly (SPACA). This compositional signature extends across the SPA basin (including to Schrödinger basin) and is likely a relict of impact melt produced by the SPA impact event (Hurwitz and Kring, 2013, 2014, 2015) or could reflect pre-impact stratification of the lunar crust (Ivanov et al., In Press).

As a consequence of its advanced age, the SPA basin interior has undergone extensive modification via processes such as impact cratering, mare/cryptomare and pyroclastic emplacement (Stuart-Alexander, 1978; Wilhelms et al., 1979; Gibson and Jolliff, 2011; Hiesinger et al., 2012; Kramer et al., 2013; Pasckert et al., 2018; Ivanov et al., In Press). Despite the thin crustal thickness across the entire SPA, the basin shows only a minor extent of volcanic activity (Wieczorek et al., 2013). A recent study from Pasckert et al. (2018) revealed the absolute model ages (AMA) of volcanic patches within SPA and found two peaks in volcanic activity. The first major peak occurred between 3.6 Ga and 3.2 Ga, which is in agreement with the timing on the nearside (Hiesinger et al., 2002, 2003) and the rest of the farside. However, the second volcanic

peak (2.2-2.5 Ga) is not observed within SPA basin. Pyroclastic material has been detected at several locations within the SPA (Wilhelms et al., 1979; Gaddis et al., 2003). Schrödinger basin has a large volcanic vent, and a fracture running north from the vent. The vent and the surrounding dark-albedo region has a high-FeO abundance compared to the surrounding basin floor material (Kramer et al., 2013). Additionally, pyroclastic materials within Antoniadi crater (Sruthi and Kumar, 2014) and potentially in the SPA basin center (Borst et al., 2012) could be found at or near the landing sites.

Additionally, an asymmetric distribution of KREEP (Potassium-Rare-Earth-Elements-Phosphorous) material was detected by the Lunar Prospector mission (Lawrence et al., 1998, 2003, 2007). The Procellarum KREEP Terrain on the nearside is enriched in heat producing elements (K, Th, U) (Korotev, 2000) which could increase melt production for volcanic activity (Wieczorek and Phillips, 2000). On the other hand, SPA has been defined by Jolliff et al. (2000) as a distinct geochemical terrane due to its intermediate Fe, and low Th signatures, which suggest the absence of a KREEP layer on the farside. Thus, there is a fundamental asymmetry in the thermal evolution of the Moon, including the distribution of heat sources in the lunar interior.

The first proposed landing site, Malapert massif, occurs along the edge of the basin while the final landing site is located near the center of the basin. As a whole, traverses planned at and around these proposed landing sites cross geologic terrains of various ages, and possibly various natures, defined by Wilhelms et al. (1979) and Spudis et al. (2008). We introduce each site in this section and provide detailed geological content of individual sites in section 5.2.

2.1. Malapert massif

Malapert massif is a mountainous surface feature located on the lunar nearside at 85.99°S, 2.93°W (Fig. 1). The massif rises ∼5 km above the lunar basal ellipsoid. Lunar massifs are postulated to form during large impact events in which underlying material is thrust above the surface creating a topographic high demarcated by faults or flexures (Harland, 2008). Thus, massifs are of particular geologic interest as they expose cross sections of the lunar crust. The ridge of Malapert massif contains two regions which are illuminated for 74% of the lunar year (Bussey et al., 2010) which may be used for solar energy collection if LER parameters allow. Additionally, the near-side (north) face of the ridge and portions of its summit are the

only regions along the 5-landing site traverse that are in constant line-of-sight communication with Earth. The area surrounding Malapert massif also contains various small-scale permanently shadowed regions (PSR) which are accessible for exploration and will provide information about extreme conditions in lunar polar environment and volatile composition.

2.2. Shackleton crater

Shackleton crater is at the South Pole (Fig. 1). It is a simple crater with a diameter of approximately 21 km at the rim and walls with slopes of ∼30° that descend to a depth of 4.2 km (Haruyama et al., 2008). The crater floor is 6.6 km in diameter and is a PSR that may contain icy deposits of volatiles suitable for in situ resource utilization (ISRU) (Mazarico et al., 2011), as well as lunar volatile-bearing regolith gardening processes. The crater walls are too steep, however, for the rovers (section 3.2) to traverse, so crew will only be able to explore the crater rim and surrounding terrain including small and large-scale PSRs. In addition to PSRs, 'cold traps' – areas whose temperatures are cold enough to host H_2O, CO_2, and other volatiles (Watson et al., 1961) – are widely distributed within the South Pole region (see Appendices A4-B5 and A4-B6).

2.3. Schrödinger basin

The landing site within the *Schrödinger basin* is located at 75°S, 133.5°E (Fig. 1). The Schrödinger basin is inside the SPA basin and formed at the end of the basin-forming epoch on the Moon (Tera et al., 1974; Cohen et al., 2000; Stöffler and Ryder, 2001; Head et al., 2010; Morbidelli et al., 2012; Orgel et al., 2018). It is the best preserved basin of its size in the Earth-Moon system. Schrödinger basin is ∼320 km in diameter, 4.5 km deep, and has a well-preserved peak ring with a diameter of ∼150 km that rises up to 2.5 km above the basin floor. The peak ring structure exposes a variety of minerals such as olivine, low and high-Ca pyroxenes, as well as anorthite (Kramer et al., 2013; Yamamoto et al., 2012). These minerals could show sequences of differentiated rock types from the upper mantle to the upper crust, respectively. Anorthosite (>97% anorthite) and pyroxene-bearing anorthosite may represent material similar to the highlands – the upper crystallization product of the magma ocean (Kramer et al., 2013). Moreover, pyroclastic material within an area of approx. 1250 km^2 with a localized source vent makes the Schrödinger basin a high-priority ISRU location (Wilhelms et al., 1979; Gaddis et al., 2003; Kramer et al., 2013).

Because it was previously identified as a high-priority site for lunar surface missions, it has received a lot of study (O'Sullivan et al., 2011; Bunte et al., 2011; Burns et al., 2013; Kramer et al., 2013; Kring et al., 2013; Kring, 2014; Kring et al., 2016; Senthil Kumar et al., 2013, 2016; Potts et al., 2015; Steenstra et al., 2016), see section 5.2.3. Samples collected from this basin can be used to address most of the science goals of the NRC (2007) report.

2.4. Antoniadi crater

The landing site within *Antoniadi crater* is located at 69.5°S, 170°W (Fig. 1). Antoniadi crater is ∼143 km in diameter with a rim-to-floor depth of 4 km. The crater is noteworthy because it contains the lowest point on the Moon. A small crater puncturing the floor of Antoniadi extends the depth to 9.2 km below the lunar basal ellipsoid (Smith et al., 2010). Antoniadi crater contains both a central peak, and a central peak ring structure and is, thus, sometimes classified as a 'proto-basin' (Dominov and Mest, 2009). This crater is an attractive site to address some of the NRC (2007) objectives (Fagan et al., 2010) due to its relatively high thorium abundance – which may be a tracer for KREEP material (Lawrence et al., 1998) – the presence of some of the youngest mare on the far side of the Moon with an AMA range from 2.2 Ga to 3.7 Ga (Wilhelms et al., 1979; Pasckert et al., 2018), and pyroclastic materials (Sruthi and Kumar, 2014).

2.5. SPA basin center

The landing site within the *SPA basin center* on the lunar farside is located at 55.4°S, 163.3°W just northeast of Bhabha crater (Fig. 1).

The proposed landing site is situated near the Mafic mound (60.0°S, 159.9°W) whose unusual composition has led to some controversy surrounding its origins – the mound may represent the remnants of SPA impact melt (Hurwitz and Kring, 2013, 2015), be an impact-induced volcanic structure, or be a hybrid of these possibilities (Moriarty and Pieters, 2015). Mafic mound is approximately 75 km long and 1 km high and is also associated with a Bouguer anomaly that implies it is associated with significant excess mass relative to its surroundings (Zuber et al., 2013). The proposed landing site is also located within the SPACA. This area has additionally been proposed to be the landing site for the MoonRise sample return mission (Jolliff et al., 2003, 2010, 2017). To the northwest of the landing site is Bose crater, which is approximately 90 km in diameter and contains a central peak and terraced crater wall. Its central peak exhibits low-Ca pyroxene that could

underlie the high-Ca pyroxene layer and also could provide impact melt from the SPA basin forming event. Additionally, pyroclastic materials from Bose and Bhabha craters may be exposed in this region (Borst et al., 2012), but unfortunately our planned traverses were not able to access these locations.

3. Concept of Operations

Here we introduce the mission architecture based on Hufenbach et al. (2015), crew rover capabilities, geologic sample requirements, and communication requirements used to develop a concept of operations.

3.1. Mission Architecture

The design reference mission scenario (Hufenbach et al., 2015) utilizes the Space Launch System (SLS), the Orion multi-purpose crew vehicle, an evolvable Deep Space Habitat (eSDH), a human lander with a reusable ascent stage, and two small pressurized rovers for crew who will be delivered to the surface for 28 days of exploration. Multiple SLS launches are needed to deliver those assets to the Moon. For this study we assume five SLS launches, one year apart, with each launch delivering a team of four crew to eDSH for subsequent surface exploration. The eDSH is a prototype habitat that builds on the expertise, capabilities, and lessons learned from the International Space Station (ISS). The conceptual vehicle has, more recently, been called the Deep Space Gateway (DSG), or the Lunar Orbital Platform-Gateway (LOP-G). In order to adhere to current nomenclature, we hereby refer to the eDSH as the LOP-G. In this DRM, the LOP-G is in a halo orbit around the second Earth-Moon LaGrange Point (EM-L2) where it will also serve as a communication relay from the lunar farside to Earth. A dual stage lander will perform descent/ascent, rendezvous, and docking maneuvres with the LOP-G. The DRM assumes the ascent vehicle can be reused up to five times, provided it receives maintenance and refueling (Hufenbach et al., 2015).

Hufenbach et al. (2015) notably uses architectural elements from NASAs cancelled Constellation program of the new millennium. The SLS is a redeveloped version of the Ares V, however, the SLS will launch both crew and cargo together rather than relying on the dual launch combination of Ares I and Ares V which were to rendez-vous in Low Earth Orbit (LEO) before continuing toward the Moon (Connolly, 2006). The Orion crew vehicle also has undergone redevelopment from the days of Constellation with the

Crew Exploration Vehicle (CEV) being modified to the Multi-Purpose Crew Vehicle (MPCV).

In terms of lunar surface scenarios, the DRM of Hufenbach et al. (2015) (and thus, the ISECG) differs from that of Constellation in that it does not establish a permanent polar outpost. The lunar habitats are instead the rovers themselves (section 3.2). The goals of "pervasive mobility" – enabling the scientific exploration of large areas of the lunar surface, "global connectivity" – enabling communication throughout exploration activities between astronauts and ground staff on Earth, and "long duration missions" – allowing comprehensive lunar exploration activities to be performed and providing a proving ground for In-Situ Resource Utilization (ISRU) and other technologies applicable for Mars exploration (Mazanek et al., 2009) – are still maintained in the Hufenbach et al. (2015) DRM.

3.2. Small Pressurized Rovers (SPR)

Two Small Pressurized Rovers (SPR) will be used to explore the lunar surface. Their design is assumed to be a flight-evolved version of the Lunar Electric Rover (LER), which has been field tested in 3-day, 14-day, and 28-day-long mission simulations (Kring, 2017; Kring et al., 2017; Eppler et al., 2013). Because we utilize the capabilities of the LER in our analysis, we will refer to the rovers as LERs rather than SPRs in the remainder of this report.

The LER utilizes the Chariot chassis of Harrison et al. (2008), which has the ability to adhere to the surface better than the Apollo Lunar Roving Vehicle (LRV). A post-Apollo analysis recommended future rovers have the capacity of ascending and descending slopes of $\sim$25° (Lunar Exploration Science Working Group, 1995). The Chariot chassis was designed to climb up 15° slope in terrestrial 1 g test conditions. When outfitted with a cabin to simulate an SPR, the LER climbed 18°-20° slopes on the flank of a cinder cone (Öhman and Kring, 2012), suggesting 25° is a reasonable limit for lunar conditions. For the present study, we adopt a maximum slope limit of 25° as a 'no-go' value, but generally plan traverses on much shallower $<$15° slopes. The average slope of our traverses is $\sim$4.3°. A summary of LER capabilities used in the study is given in Table 1. We also note that the slope is generally downhill from the first landing site at Malapert massif to the SPA basin center (Fig. 4).

LERs may be operated by crew around landing sites and tele-robotically from the LOP-G or Earth(via the LOP-G or satellite relay) between landing sites. When crewed, the LERs typically accommodate two crew members,

Table 1: Summary table of concept of operations

Characteristics	Tele-robotic operation	Crew operation
Average speed	0.36 km/hr (0.1 m/s)	5 km/hr (1.38 m/s)
Maximum slope	25°	25°
Preferred slope	under 15°	under 15°
Driving capability	only sunlit periods	sunlit periods and lunar darkness
Driving limitation	only during direct communication with Earth	max. 14-days

however, in the event of an emergency a single LER is capable of supporting all four crew members for a limited time. As per simulations carried out during NASAs Desert Research and Technology Studies (DRATS) simulations in Northern Arizona (Eppler et al., 2013), crew may conduct LER-enabled traverses away from the landing site for a maximum of 14 days – this number reflects the total volume of consumables that can be carried by the rover. Each LER is equipped with a Portable Utility Pallet (PUP) – a portable charging station that also provides exterior storage for consumables, and a Portable Communications Terminal (PCT) to provide additional communications flexibility when crew are performing Extra-Vehicular Activities (EVA).

The LER is also a geological tool that accommodates Intra-Vehicular Activity (IVA) (Kring, 2017; Kring et al., 2017). It includes high-visibility windows that provide a 180° field-of-view and incorporates a minimum of six cameras – ForeCam, AftCam, port and starboard cameras, and docking cameras – which are utilized for safety, traversing and scientific purposes. These features facilitate observations and imagery of both local and distant geological features. The DRATS simulation illustrated that IVA could provide high quality scientific characterization, similar to those enabled by EVA. EVA capability incorporates a SuitCam, enables mobile observations, and allows for in-situ sampling which is assisted using the onboard geologic tool rack which contains rock hammers, tongs, a scoop, sample bags, and a sample storage compartment. Without accurate estimations of the reduced productivity of the LERs during lunar darkness, this study assumes the same rate of both IVA and EVA ability for daytime and night-time operations. There is a need for a trade study which investigates both driving and sampling (section 3.3) in limited illumination conditions (section 6).

At the time of this study, several uncertainties remain regarding the instrumentation payload that will be employed on the LER. Table 2 provides an overview of NRC (2007) goals that could be addressed along each 'between landing site traverse' if each of the additional notional instruments

were included. The instruments considered for this study are adapted from Steenstra et al. (2016) who utilzed the HERACLES mission concept, they are: Ground Penetrating Radar (GPR) – for lateral and vertical subsurface structure observations (we assume this is deployed at every landing site), a GigaPan camera – which provides oblique, color images at gigapixel resolution for panoramic and detailed visualization of geologic features of interest, an Alpha Particle X-Ray Spectrometer (APXS) and a Laser Induced Breakdown Spectrometer (LIBS) – for in-situ chemical analyzes, and a neutron spectrometer to detect H-bearing volatiles. Although we did not assume the LER would have a robotic arm for sample collecting, it became clear during the course of our study that an arm and ability to collect samples would greatly enhance our ability to address NRC (2007) science objectives and ISRU objectives.

A notable advantage of conducting either tele-robotic or crewed traverses with the LERs is that close-up imagery of exposed stratigraphy can be captured with the range of cameras onboard – particularly the Gigapan – which can provide high-resolution detail about exposures on side-facing slopes which are not visible in orbital imagery.

Table 2: NRC(2007) goals addressed with the addition of notional instrumentation to the LER. See Appendix A5 for a breakdown of all NRC goals.

Unit Type	NRC Goals (GPR)	NRC Goals (Chem. Analysis/APSX)	NRC Goals (Gigapan)	Neutron Detector
Simple crater	3d, 6a, 6c, 6d	3a, 3b, 3c, 3d, 6a, 6c, 6d, 7a	2a, 3d, 3e, 6a, 6b, 6c	
Complex crater	3d, 6a, 6b, 6c, 6d	3a, 3b, 3c, 3d, 6a, 6b, 6c, 6d, 7a	2a, 3d, 3e, 6a, 6b, 6c	
Ejecta blanket	3d, 6b, 6d	3d, 6d	3d, 6b	
Impact melt sheet	3d, 6a	3d, 6a	2a, 3d, 6a	
Megaregolith	3d, 3e	3d, 3e	3d, 3e	
Regolith	3d, 4e, 7a, 7b, 7c	3d, 7a, 7b, 7c, 7d	2a, 3d	
Volatiles	3d, 4a, 4c, 4d	3d,	3d	4a, 4b, 4c
Pyroclastic material	3d, 5c	3d, 5c	2a, 3d	
Mare deposit	3d, 5a	2d, 3a, 3d, 5a, 5d, 6c	2a, 3d	

The LER is designed to travel at speeds up to 5.56 m/s (20 km/hr) (Harrison et al., 2008), approximately twice the maximum designed speed of an Apollo-era LRV (Costes et al., 1972). Speeds adopted for use in this study are 1.39 m/s (5 km/hr) for crewed traverses, and 0.1 m/s (0.36 km/hr) for tele-operated traverses. The reduced speed for tele-operations will make it easier to avoid hazards and, importantly, will allow for continuous subsurface surveys with a GPR and volatile detection with a neutron spectrometer.

3.3. Sampling Requirements

When tele-robotically operated between human landing sites, the LER – at its current stage of development – has no sample collection ability. We show in Table 2 and in Section 5.1 that such an ability may be warranted given the terrain traversed and the number of NRC (2007) objectives these samples may address. This information is also presented in detailed tabular form in Appendix A1. When LERs are crewed at landing sites, sample collection is possible via EVA – the NRC (2007) objectives able to be addressed at each site are discussed in detail in section 5.2 and a detailed summary of all planned EVAs (location, addressed NRC (2007) objectives, sample types, sample masses) is presented in Appendices A2-A to A2-E.

A key constraint when estimating total sample mass requirements for the EVAs mentioned above concerns the complexity of lunar geology. The rock type and analytical methods suitable for that rock type dictate the sample size required to address any given science goal. Here we estimate minimum samples masses using parameters recommended by the Curation and Analysis Planning Team for Extraterrestrial Materials (CAPTEM) (Shearer et al., 2007). For example, CAPTEM (their Table 5) recommends 500 g for a mare basalt sample, 5000 g for a complex impact breccia, 0.5 g/clast for a rake sample, and 2000 g for an unsieved regolith sample. As each lithology is encountered in our traverses, sample masses are collected using those guidelines (Table 3).

An alternative way to estimate sample mass is by using a sampling rate per EVA hour. An analysis of Apollo missions determined that the astronauts collected 2.3 kg per crew member per EVA hour (Kring, 2007). Applying that metric, our traverses would produce larger masses than those estimated using minimum CAPTEM recommendations (Table 4). In this table, sample masses are also given in the case that only a single LER crew goes EVA each day.

3.4. Communications

When assessing the feasibility of communications coverage for this study we considered several options: direct Earth-Moon-Earth communications achieved via radio communications, based on calculations performed by Massachusetts Institute of Technology (2016), Earth-Moon-Earth communications using a relay tower on Malapert massif, and Earth-Moon-Earth communications using the LOP-G at EM-L2.

Table 3: Summary of minimum sample masses collected for traverses at each site in this study. These are minimum sample masses because they assume only a single sample of each type is collected per station using CAPTEM recommendations (Shearer et al., 2007). In reality, multiple samples are likely.

Sample Type (collection method)	Malapert massif	South Pole (Shackleton crater)	Schrödinger basin	Antoniadi crater	SPA basin center
Pyroclastic material (scoop)	-	-	10	14	-
Pyroclastic material (hand specimen)	-	-	-	3.5	-
Peak ring/central peak material (hand specimen)	-	4	2.5	1.5	1
Mafic mound (hand specimen, breccia)	-	-	-	-	15
Mare/cryptomare basalt (hand specimen)	-	-	1.5	4	2
Impact melt (breccia, hand specimen)	55	1.5	35	45	25
Wall material (breccia, rake)	-	-	23	1.5	20
Ejecta (rake, scoop, breccia)	26	-	4	5	11
Volatile-rich regolith (scoop)	16	36	2	-	-
Regolith (scoop)	34	5	10	8	16
Total (kg)	126	46.5	88	82.5	90

Table 4: Sample masses per landing site calculated using a sampling rate of 2.3 kg per crew member per EVA hour (Kring, 2007). The number of EVA at each landing site are 24, 18, 34, 23, and 18 respectively.

	Sample Mass (kg) at each landing site				
Collection rates	Malapert massif	South Pole (Shackleton crater)	Schrödinger basin	Antoniadi crater	SPA basin center
Four crew members (9.936 kg/hr)	238.5	178.8	337.8	228.5	178.8
Two crew members (4.968 kg/hr)	119.2	89.4	168.9	114.3	89.4

The north-facing ridge of Malapert massif and portions of its summit are the only regions along the 5-landing-site traverse that are in direct line-of-sight communication with Earth. The south-facing side of the massif, as well as much of the region south of the massif (traversing toward the lunar farside) cannot be in direct contact with Earth as they are shielded by the topography of the massif. See Appendix A3 for details of communications scenarios using the direct-to-Earth methods tested in this study.

For a humans-to-surface mission, continuous contact with Earth is desired and, thus, we select a halo orbit around EM-L2 (Hopkins et al., 2013). Hopkins et al. (2013) states that there are two broad classes of halo orbit available, a northern-class halo, which spends more time over the northern hemisphere of the Moon, and a southern-class halo, which spends more time over the southern hemisphere of the Moon. Of these two classes, the southern-class is the most suitable for observation of all of the proposed landing sites in the south polar region. Another important consideration in selecting an orbital configuration for all proposed landing sites is the amount of coverage at each site. Thus, there are two additional orbital sub-configurations to be considered – small and large halos. Large halos are positioned further

Table 5: Communication coverage at landing sites utilizing a relay in a halo EM-L2 configuration. The calculated values are provided by Lockheed Martin (2016), based on a previously published analysis for a small halo orbital period of 14.8 days and a large halo orbital period of 10.6 days (Hopkins et al., 2013).

Proposed Landing Site	Small Halo (days / % coverage)	Large Halo (days / % coverage)
Malapert massif	2.96 / 20-30	8.90 / 84
Shackleton crater	4.44 / 30-40	8.90 / 84
Schrödinger basin	11.84 / 60-90	9.01 / 84-85
Antoniadi crater	14.80 / 100	9.01 / 85
South Pole-Aitken basin center	14.80 / 100	9.12 / 85-86

from EM-L2 and closer to the Moon, giving them an orbital period of approximately 9 days, while small halos are positioned closer to the EM-L2 point, which increases the length of their orbital period to approximately 14.8 days (Hopkins et al., 2013). As seen in Figure 2 the large southern-class halo provides consistent coverage of the majority of our proposed landing sites Lockheed Martin (2016). The small southern-class halo provides superior coverage for three of out five sites, however, Malapert massif and the Shackleton crater experience severely reduced coverage, with only 2.96 and 4.44 days of communication respectively, see Table 5. Therefore, using the Hufenbach et al. (2015) architecture, the LOP-G would be placed into the large southern-class configuration.

Though not pursued in this study, another feasible option is to place the LOP-G into a Near Rectilinear Halo Orbit (NRHO) using DRM architecture from Whitley et al. (2017). If the NRHO were selected as the orbital configuration for the LOP-G in this study up to 86% coverage for all landing sites would be possible (Whitley and Martinez, 2016), an improvement of up to 2% coverage at four of the five proposed landing sites. While the NRHO is comparable to the large and small halo configurations in terms of propellant cost, this configuration offers additional advantages in that it has very short transfer times (0.5 day vs 3 days for an EM-L2 halo), reducing crew time on the landing vehicle, decreasing the mass required for air, supplies and related systems, and allowing for an increase in propellant mass (Whitley et al., 2017).

4. Methodology

We design telerobotic traverses between landing sites and crew traverses at landing sites in ESRI ArcGIS© 10.1. Trafficability information is obtained by deriving slope maps and hillshaded Digital Elevation Models (DEM) from Lunar Orbiter Laser Altimeter (LOLA) (Smith et al., 2010) data available at resolutions from 10 to 100 m depending on latitude latitude (Malapert massif: 20 m/pix, South Pole/Shackleton 10 m/pix, Schrödinger basin and Antoniadi crater: 60 m/pix and SPA basin center: 100 m/pix). Slope profiles were derived using LOLA DEM at resolutions from 10 to 100 m/pix (Appendix A4-A1, A4-B2, A4-B3, A4-C4, A4-C5, A4-C6, A4-D2, A4-D3). 3-D visualizations of landing site accessibility are created in ArcScene© by combining Lunar Reconnaissance Orbiter (LROC) (Chin et al., 2007) Narrow Angle Camera (NAC) (1m/pix) imagery with LOLA DEMs at 60m/pix resolution for Schrödinger basin and Antoniadi crater. We processed these raw NAC images using the Ames Stereo Pipeline (Moratto et al., 2010).

To assess notional traverses, LROC Wide Angle Camera (WAC) (100 m/pix) images are overlaid with a selection of geologic maps (Wilhelms et al., 1979; Spudis et al., 2008; Gibson and Jolliff, 2011; Borst et al., 2012; Kramer et al., 2013; Sruthi and Kumar, 2014) in order to optimally locate sampling stations. Furthermore, we use these maps and their associated literature to identify scientifically interesting geologic features to visit en route. Additional data are extracted from Sruthi and Kumar (2014) and Kramer et al. (2013) concerning boulder availability and volcanic cones for Antoniadi crater, and M^3 (Green et al., 2011) spectral data for Schrödinger basin. LROC NAC images are used to refine station locations to specific deposits, outcrops, contacts, or boulders, as well as avoid hazards such as small craters below the detectable resolution of existing regional DEMs. Sample collection is designed in order to maximize the number of NRC (2007) concepts and goals that can be addressed at each site and across the study as a whole.

To obtain information about lunar volatile and cold-trap locations we use various datasets (Paige et al., 2010; Mazarico et al., 2011; Mandt et al., 2016). In order to identify regions where H_2O and CO_2 ice are present, temperature data from LROs Diviner Lunar Radiometer Experiment is used (Paige et al., 2010). This data includes maximum, average, and minimum annual surface temperatures at 240 m/pix resolution. ArcGIS© was used to create binary raster data indicating areas where H_2O and CO_2 ice can be stable. The H_2O ice stability map (Appendix A4-B5) is created based on

regions where temperatures are lower than the H_2O sublimation temperature of 106° K, and CO_2 ice stability map (Appendix A4-B6) is based on areas where temperatures are lower than the CO_2 sublimation point of 54°K (Zhang and Paige, 2009, 2010). We use a map of permanently shadowed regions from Mazarico et al. (2011) at a resolution of 240 m/pix (Appendix A4-B4). We also derive hydrogen concentration maps in 100 ppm, 125 ppm, and 150 ppm from Lunar Prospector Neutron Spectrometer (NS) data (Appendix A4-B5) Elphic et al. (2007).

Traverse routes were located between the refined sampling stations using a least cost approach with a high weight given to the slope dataset in order to adhere to the slope capabilities of the LERs.

5. Results

5.1. Tele-Robotic Traverses Between Landing Sites

This section considers the feasibility of traversing between human landing sites in the allotted traverse period of one year between crew landings (Hufenbach et al., 2015). As illustrated below, we found that it is possible for LER to navigate from the first landing site to the fifth landing site, although access to the floor of Antoniadi crater and one of two potential access routes to the floor of the Schrödinger basin need to be confirmed.

For between site traverses, we design two types of traverse to fully investigate potential options; a 'direct' traverse, and a 'science' traverse (Fig. 3). The first utilizes the most direct route between human landing sites (given the slope capabilities of the LERs) and, thus, takes much less time to complete. Through examination of multiple datasets along these direct routes we determine that no additional observational/sampling opportunities exist that provide information (with respect to the NRC (2007) concepts) that we do not already address with the at-landing site traverses. Thus, no time is allocated for observation along these routes and the LERs arrive at the next landing site early and sit waiting for the arrival of the next crew for up to several months.

The second type of traverse, the 'science' traverse, takes into account additional scientific gains that could be made if the entire year were utilized for observation and potential sampling (depending on notional LER instrumentation). Thus, science traverses deviate from the direct traverse routes in order to travel longer distances to sites of interest that may offer additional scientific merit with respect to the NRC (2007) concepts. For these

traverses, we also consider deployment of notional instrumentation that may offer scientific gain if included on the LER; see section 3.

With respect to risk, these science traverses are designed with slope and terrain factors in mind, as well as the 365-day travel time constraint; see Figure 4 for an overview of the route, in which it can be seen that the entire travel route progresses downhill into the basin center. With respect to the travel time constraint, the total driving time for the LERs is further limited by communications coverage (see section 3.4), which may not be continuous, as they are to be tele-operated between human landing sites.

We assume that the surface is illuminated for 50% of the year (simply due to the day/night transition), and that the LERs will only be tele-operated in the daytime to maximize hazard avoidance. We then use communication data from Lockheed Martin (2016) to calculate maximum driving times for each traverse given orbital coverage for each landing site (Table 6 and Fig. 2). The maximum driving distance is then calculated by multiplying this number with the allowable speed of the LERs while tele-operated (0.1 m/s or 0.36 km/hr). An assumed contingency margin of 30% is taken into account along all traverses, which is also subtracted from the maximum number of possible driving days. As a result, this provides the 'safe' driving distance (due to full communications and hazard avoidance) for the traverses between human landing sites in one year (see Table 6).

Table 6: Direct and science traverse lengths with respect to 'safe' driving distance with the LER tele-operated from EM-L2.

From	To	'Safe' Distance (km)	Direct Traverse (km)	Direct Traverse Time (days)	Science Traverse (km)	Science Traverse Time (days)
Malapert massif	South Pole/Shackleton crater	932.7	208.4	24	911.4	105
South Pole/Shackleton crater	Schrödinger basin	938.2	739.7	86	923.5	106.8
Schrödinger basin	Antoniadi crater	943.7	681.9	79	935.9	108
Antoniadi crater	South Pole-Aitken basin Interior	949.2	939.5	108	946.9	109

Detailed tables for each 'science' traverse are available in Appendix A1, documenting potential sampling stations, geologic units, and NRC (2007) goals able to be addressed with cameras, with sample return and with additional instruments. Note that in this study we find no opportunity to explore lava tubes during tele-robotic traverses between landing sites, or crewed traverses at and around landing sites.

Slope profiles for each of the direct and science traverses are given in Appendix A6.

5.1.1. Malapert Massif to Shackleton Crater

The direct and science traverses from Malapert massif to Shackleton crater are presented in Figure 5.

The direct traverse lies south of the Malapert massif, circumnavigates Haworth crater in a clock-wise direction, and passes the western rim of Shoemaker crater before approaching the South Pole/Shackleton crater landing site. It is 208.4 km in length and takes ∼24 days (579 hrs) to complete. This leaves a 93% (331 day) contingency margin for the first long-distance, tele-operated LER direct traverse. The average slope across the entire traverse is 5.2° (Appendix A6).

The science traverse passes through Cabeus crater, which is one of the most critical sites for studying the distribution and composition of volatiles and the Moon. Cabeus crater contains one of only three large PSRs in the southern region which exhibit epithermal neutron suppression – suggestive of high hydrogen abundance and water ice deposits (Sanin et al., 2012). The Lunar Prospector Neutron Detector measured a high concentration of hydrogen in Cabeus crater (Elphic et al., 2007), while the impact of the Lunar Crater Observation and Sensing Satellite (LCROSS) at this location caused an impact generated plume where the total water, ice and vapor was estimated to be 3-4% (Colaprete et al., 2010). Additionally, LROs Diviner Lunar Radiometer Experiment recorded temperatures that suggest the PSRs within Cabeus could host CO_2 ice (Paige et al., 2010). During the traverse, multiple GPR and neutron detector measurements across Cabeus crater's floor can help provide an understanding of the lateral and vertical distribution of lunar volatiles at this much studied location and broadly address NRC (2007) Concepts 4 and 7.

Using imagery from the LERs onboard optical cameras, or a Gigapan, stratified outcrops can also be studied in detail. As the traverse progresses through Cabeus, Drygleski and Ashbrook craters, images can help obtain a better understanding of the complexity of the current lunar crust, and determine the structure of multi-ring impact basins (NRC (2007) Concepts 3, and 6). Due to time constraints previously discussed, the LERs will only traverse along the rim of Drygleski crater rather than visit its central peak to remain within 'safe' driving distance.

The science traverse is 911.4 km in length, and takes ∼105 days (2532 hrs) to complete. This leaves a ∼70% (250 day) contingency margin for the first long-distance, tele-operated LER science traverse. The average slope

across the entire traverse is 5.4° (Appendix A6).

5.1.2. Shackleton Crater to Schrödinger basin

The direct and science traverses from Shackleton crater to Schrödinger basin are presented in Figure 6.

The direct traverse travels south in an anti-clockwise direction from the landing site nearby Shackleton crater before progressing north (once the limb and pole is crossed) to an access point in the southern rim of Schrödinger basin and terminates at the landing site beside a pyroclastic vent. The direct traverse is 739.7 km long and takes ∼86 days (1894 hrs) to complete. The average slope across the entire traverse is 3.6° (Appendix A6).

The science traverse departs the landing site near Shackleton crater and travels south in a clockwise direction before crossing the nearside/farside boundary. The traverse then moves west toward Amundsen crater which has been proposed as an interesting site for the study of lunar volatiles (Lemelin et al., 2014; Runyon et al., 2012) as the relatively low slope of the crater facilitates LER access. Temperatures within PSRs in this region were measured with LROs Diviner instrument and it was observed that specific sites within these PSRs contain maximum temperatures that do not exceed 54°K (see Appendices A4-B5 and A4-B6). This implies that Amundsen crater is one of the few areas in the south polar region where CO_2 ice may be found (Fig. 7); thus it provides an opportunity to examine the lateral composition and distribution of lunar volatiles and provide additional valuable information to address NRC (2007) Concept 4.

With respect to geology, as Amundsen crater is classified as a complex crater its central peak is of particular interest, because it may contain uplifted basement material (Runyon et al., 2012) (NRC (2007) Concept 3). Estimates of the original depth of this excavated material are currently dependent on the equation used to summarize uplift. For example, using the depth of melting of Cintala and Grieve (1998) material may have been excavated from approx. 16 kms. Using a stratigraphic uplift equation from Kring and Durda (2012) may return values of approx. 18 km. Thus, it is sensible to estimate that material exposed in central peaks could originate from depths greater than 15 km. Sampling of this material will help to refine its age. Impact melt from Amundsen will also be sampled so age determination can be performed in order to calibrate the impact flux rate (Kring, 2014) (NRC (2007) Concept 1).

Additionally, this traverse visits some geological contacts from different

epochs around Shackleton, such as Imbrian plains, and pre-Nectarian crater material (Spudis et al., 2008). These may be studied by direct sampling or through chemical measurements and analysis.

Trafficability measurements from NAC images, in combination with a 60 m LOLA DEM (Fig. 8) and the slope map in Appendix A4-C3, are used to identify two ingress/egress points on the southern and eastern rim. To minimize driving distances, the southern access point is used to access the basin floor en route from the South Pole and the other is used to depart en route to Antoniadi crater. The southern ingress point is particularly challenging (Fig. 6), but seems feasible based on slope limits. Nonetheless, this ingress point will need to be verified with additional study (section 6). If this ingress point becomes suspect, then the LERs can access the basin floor from the east. That will, however, reduce the time available for the LERs to survey the floor of Amundsen crater between the South Pole and the Schrödinger basin.

The science traverse is 923.5 km in length and takes ∼106.8 days (2563.2 hrs) to complete. The average slope across the entire traverse is 4.3° (Appendix A6).

5.1.3. Schrödinger Basin to Antoniadi Crater

The direct and science traverses from Schrödinger basin to Antoniadi crater are presented in Figure 9.

The direct traverse exits Schrödinger basin through the eastern rim and travels in a northeastern direction to Antoniadi crater following the most direct path of lowest slope. The direct traverse is 681.9 km in length and takes ∼79 days (1894 hrs) to complete. The average slope across the entire traverse is 3.7° (Appendix A6).

The scientific traverse from Schrödinger basin to Antoniadi crater follows the path of the direct traverse exiting Schrödinger. It then diverges in a northerly direction to study excavated material in the vicinity of the basin. In particular, this traverse targets the secondary crater field from Antoniadi crater and impact melt ponds of Schrödinger basin as described by Kramer et al. (2013) (NRC (2007) Concept 1). The traverse then travels east, rejoining the direct traverse to enter Antoniadi crater from the south. Along this traverse the walls of both Schrödinger basin and Antoniadi crater will also be studied because they have the potential to contain stratification of the SPA melt sheet (NRC (2007) Concept 6).

As in section 5.1.2, we use trafficability measurements from NAC images,

in combination with a 60 m LOLA DEM and the slope map in Appendix A4-D1B to identify an ingress point into Antoniadi crater through its southern rim (Fig. 10).

The science traverse is 935.9 km in length and takes ∼108 days (2599 hrs) to complete. The average slope across the entire traverse is 4.2° (Appendix A6).

5.1.4. Antoniadi Crater to South Pole–Aitken Basin Center

The direct and science traverses from Antoniadi crater to the South Pole-Aitken basin center are presented in Figure 11.

The direct traverse from Antoniadi crater to the South Pole-Aitken basin center leaves Antoniadi from the access point on its southern rim and progresses north through the interior of Berlage crater before continuing toward the fifth human landing site. The total length of the traverse is 939.5 km, it takes ∼108 days (2609 hrs) to complete. The average slope across the entire traverse is 4.4° (Appendix A6).

The science traverse from Antoniadi crater to SPA basin center does not allow for much extra science exploration due to the driving time constraints mentioned in the introduction to this section. The only divergence from the direct traverse occurs while approaching Mafic mound, as the science traverse approaches from a different direction. This allows for further science observations to be made that can provide additional information to constrain the origins of Mafic mound. If it consists of melt sheet from SPA, it can be used to determine the age of this basin (NRC (2007) Concepts 1 and 3). Mare basalts and cryptomare can be studied closer to the SPA basin center landing site and will therefore provide a better understanding of the age of volcanic events on the lunar farside (NRC (2007) Concepts 3 and 5). The science traverse is the longest of all between site traverses, with a length of 946.9 km which takes ∼109 days (2630 hrs) to complete. The average slope across the entire traverse is 4.5° (Appendix A6).

5.2. Crew Traverses At and Around Landing Sites

For four of the five landing sites, we designed two traverses to address National Research Council (2007) and to illuminate issues that need to be addressed by additional studies. Each traverse is <14 days long and is a loop that brings the crew back to the landing site either to restock consumables for subsequent traverse loops, or to return to the LOP-G. Potentially, one loop could be done in a 14-day-long sunlit period and the other in darkness, during

a 28-day-long mission. If it is determined that crew cannot operate the LER during darkness, then either one of the loops could be chosen for daytime operations. For extended 42-day missions, e.g., as identified in the current edition of the Global Exploration Roadmap (International Space Exploration Coordination Group, 2018), both traverse loops can be conducted in sunlight within an intervening night-time stay at the landing site. We designed a 40-day, three loop traverse for Schrödinger basin to explore this option, leaving 2-days of contingency margin.

The rest of this section is structured as follows: for the first human landing site at Malapert massif, we fully describe its scientific potential, constituent traverse loops, slope profiles, individual sampling stations, and sample collection information in the main text, and refer readers to the corresponding attribute table for this landing site in Appendix A2-A. For subsequent human landing sites all detailed traverse information such as traverse loops, sampling stations, recommended samples, collection methods and masses, as well as the NRC (2007) concepts and the individual goals these samples address are given in their respective attribute tables available as individual appendices, see Appendices A2-B, A2-C, A2-D, and A2-E. Those traverses will only be broadly described in the main text. Note that in figures where the field-of-view allows, an exploration zone with a Mars-forward radius of 100 km from the landing site is outlined in white. We also calculate approximate times needed for each traverse given landing site setup and breakdown operations, LER driving speeds, communication coverage requirements, and an EVA time allowance of approximately 1 hour for each sampling station. A tabular visualization of all NRC concepts and goals addressed at each landing site is provided in Appendix A5.

We assume that after initial descent onto the lunar surface (at the first human landing site) LERs need to be deployed from their stowed position on the lander, have their systems activated and checked, and be stocked with consumables. In addition, the lander may be prepared for hibernation while crew are completing traverses. Notional time allocations for these logistics are presented for the Schrödinger basin site in Appendix A4-C2.

5.2.1. Malapert Massif Traverse

As discussed in section 2, Malapert massif is a mountainous surface feature located on the lunar nearside at 85.99°S, 2.93°W (Fig. 1). The landing site for Malapert massif is situated on a flat area of high albedo on its western flank. Figure 12 shows the proposed dual loop Malapert massif traverse

overlain on a 20 m/pix LOLA DEM.

In terms of geology, Figure 13A contains the Spudis et al. (2008) geologic map overlain over a 20 m/pix hillshaded elevation model. From this Figure, it can be seen that Traverse 1 (Stations 1-12) crosses four distinct terrains, including pre-Nectarian terra material, pre-Nectarian massif material, pre-Nectarian platform massif material, and Orientale basin secondary crater material. Traverse 2 (Stations 13-24) additionally crosses 7 distinct geological terrains: pre-Nectarian terra material, pre-Nectarian massif material, pre-Nectarian crater materials, Imbrian crater materials, Imbrium basin secondary crater material, pre-Nectarian platform massif material, and Orientale basin secondary crater material (Spudis et al., 2008). Samples are collected from each of these terrains in order to better constrain lunar chronology.

Figure 13B shows the proposed Malapert massif traverse overlain on a 20 m/pixel slope map to illustrate the LER access between stations. These average values are under the preferred slope of 15°, and the maximums are below the LER slope constraint of 25°. If adherence to smaller slope values becomes necessary, future study is required to pinpoint the locations of 'choke points' along the traverses planned in this study.

These 'choke points' are regions along the traverse in which slopes are highest (according to the 20 m/pixel slope maps) and care must be taken to traverse these points in the LER. However, none of these regions are above the LER slope constraint value of 25°. A slope profile for the first loop of the Malapert traverse is presented in Fig. 14, which shows that regions of high slope (>15°) are concentrated approaching Malapert ridge (Stations 1, 2, 3, and 4) – if these regions were unable to be traversed access to the ridge would not be possible and observation of massif structure, as well as highly illuminated regions, would be lost (see Traverse Loop 1 section below). To address this issue, in future studies higher resolution DEMs need to be constructed from LROC NAC images (1 m/pixel) in order to calculate slopes more accurately and pinpoint the locations of 'choke points' at the scale of the LER, as it is possible there may be room to maneuver around them given finer scale information.

Figure 13C shows the locations of PSRs in and around the proposed Malapert massif traverse. Sampling stations have been positioned to collect volatile-rich regolith within several of these regions to address NRC (2007) Concept 4. Additionally, along the ridge of the massif are two regions which experience constant illumination for 74% of the lunar year, these are referred

to in Bussey et al. (2010) and De Rosa et al. (2012) as points M1 (86.04°S, 2.7°E) and M2 (86.00°S, 2.9°W). These sites may be utilized for solar energy collection if LER parameters allow, as they are located on slopes of 20-25° (M1) and 15-20° (M2) respectively, midway between Stations 1 and 2. These highly illuminated regions provide excellent locations for the collection of solar energy, as solar arrays placed in these regions have the potential to support the power requirements of short-term missions. For longer-term exploration, permanent infrastructure could be established in these locations to provide long-term support. For this study, flexible exploration time has been allocated to deploy the Portable Utility Pallet (PUP) onboard the LERs for solar energy collection at these sites if required.

Based on communication calculations provided by Lockheed Martin (2016) the Malapert region receives coverage for only 84% (8.9 days) of a single 10.6 day orbital period; see Table 5 and Figure 2A. During the 1.7 day communication dropout, crewed LERs cease all exploration activities and remain at their current station until the next orbital period begins and coverage is regained. These communication pauses have been integrated into the total times calculated for Traverses 1 and 2.

Broadly speaking, traversing the Malapert massif region allows the NRC (2007) Concepts 1, 2, 3, 4, 6, and 7 to be addressed (Appendix A5-A).

Traverse Loop 1. Figure 12 illustrates a traverse loop that extends broadly east from the landing site up over the ridge onto the peak of Malapert massif where four EVA stations are to be located (Stations 1, 2, 3, 4). EVAs at these stations will involve the sample collection of massif material and observations of massif structure. The two regions of 74% illumination between Stations 1 and 2 can also be investigated with allocated flexible exploration time, and the PUP deployed for collection of solar energy. If Ground Penetrating Radar (GPR) is included on board the LER it will be used at Station 3, located on the peak of the massif. GPR can gather structural information about the subsurface to varying depths depending on its frequency (Xiao et al., 2015) and can address goals within NRC (2007) Concepts 2 and 3. Due to the topography of the massif and slopes along the ridge the only path off the massif retraces the ascent path taken by the LERs. Once the LERs have returned to the vicinity of the landing site the traverse continues westward, traveling to the twin craters located on the massif adjacent to Cabeus crater. Sample collection of regolith and impact ejecta will be performed at Stations 5 and 6 on this traverse path before the twin craters are reached, and the

structure of this secondary massif will be observed and documented using GigaPan imagery addressing NRC (2007) Concepts 3, 6, and 7.

The twin craters, mapped as secondaries from Orientale basin event (Spudis et al., 2008), will have samples collected from their rims at Stations 7 and 8. Collection of impact-reset lithologies associated with these craters may help provide an age for the Orientale impact addressing goals within NRC (2007) Concept 1.

The traverse continues south before making its way back to the landing site, traversing across the secondary massif by Cabeus crater and sampling volatile-rich regolith from a PSR location (Station 9, Station 11, Station 12), as well as crater ejecta and regolith samples (Station 10). Sampling of PSRs and regolith can broadly address NRC (2007) Concepts 4 and 7. Observations of massif structure will be taken at these stations, broadly addressing NRC (2007) Concept 6.

Traverse 1 is approximately 206.8 km long, taking a total of 10 days (64.0 hours) to complete with the inclusion of 12 EVA stations. It has an average slope of 6.8°, and a maximum slope of 19.2°. Making additional time allowances for communication dropout during each orbital pass, the total traverse time is approximately 12 days. Additionally, this traverse has been notionally planned to take place during the lunar night and it is the initial human landing site using the proposed architecture, an additional two working days (15 hours) of margin have been allocated to allow for reduced exploration speeds bringing the total time taken for this traverse to 14 days. However, if it is determined that crew cannot operate the LER during lunar night, then this loop may be scheduled to occur in lunar daytime. As previously mentioned, the feasibility of night-time operations needs to be addressed by additional studies.

Traverse Loop 2. The second traverse loop travels to a large impact crater north of Malapert massif. At this station sample collection of impact-reset lithologies can test the hypothesis that it is a secondary crater of the Imbrium basin-forming impact event (Spudis et al., 2008). Observations and potential sampling of ejecta associated with this crater will help to constrain models of secondary crater production and its effect on regolith mixing answering goals within NRC (2007) Concepts 1, 3, 6, and 7. The traverse continues east toward a small crater chain from which an ejected block can be collected (Station 14). This sample may be suitable for cosmogenic nuclide studies which can help provide an age determination for the impact event by constraining

the effects of space weathering and the flux of solar radiation with time.

Nearby, at Station 15 samples of volatile-rich regolith will be taken across a PSR boundary. This can help address the changes in composition throughout the transition from volatile-rich to typical lunar regolith. Additionally, impact melt breccia will be collected at this station. NRC (2007) Concepts 1, 3, 4, 6, and 7 are addressed at stations in this region. Additionally, as the traverse is bounded on the east by the Leibnitz Beta plateau, sampling of this third massif structure is possible at two stations (16 and 17). From each station, regolith, massif, impact melt breccia material or volatile-rich regolith will be collected. Observations of the massif structure and stratigraphy will also be documented collected via GigaPan imagery. Samples from these stations can address goals from NRC (2007) Concepts 3, 6, and 7.

Stations 18, 19, and 20, which are on the south side of Malapert massif address the collection of volatile-rich regolith from PSR, excavated components from the Haworth impact, and the observation of Malapert massif structure (NRC (2007) Concepts 3, 4, 6, 7). Stations 21 and 22 overlooking Haworth crater will sample the impact-reset lithologies from the crater, providing one of the first ages of a pre-Nectarian impact crater and addressing NRC (2007) Concept 1. Excavated components entrained in impact breccia may provide a measure of lithological variation in the lunar crust addressing NRC (2007) Concept 3. Additionally, because of Haworth's significant excavation depth, it has the potential to provide information about the vertical extent and structure of the megaregolith, which will be documented using the GigaPan imagery, and broadly address NRC Concepts 3 and 6. PSRs will also be sampled here, addressing Concepts 4 and 7. Final EVA stations along this route will sample massif material and documenting the structure of the western edge of Malapert massif, and additionally sample volatile-rich regolith from small PSR, addressing NRC Concepts 3, 4 and 7.

Traverse 2 is approximately 282.8 km long, taking a total of 12 days (83.6 hours) to complete with the inclusion of 12 EVA stations. It has an average slope of 5.6°, and a maximum slope of 19.5°, see Appendix A4-A1. Allowing for communications dropout during an EM-L2 orbital pass, the traverse takes 14 days. Traverse 2 is envisaged to take place within the duration of a lunar day to maximize the quality of stratigraphic Gigapan imaging, however, the feasibility of crew operations within lunar darkness needs to be studied.

These two Malapert area traverses are, in general, similar to those designed for Lunar Surface Systems during NASA's Constellation Program (Kring, 2011), which were then used for a 28-day-long, dual LER lunar

mission simulation during NASA's Desert Research and Technology Studies (DRATS) campaign of late 2010.

5.2.2. South Pole (Shackleton Crater)

From Figure 15 it can be seen that Shackleton crater descends to a depth of approximately 4.2 km and its inner walls are fairly steep, with slopes of approximately 30° (Haruyama et al., 2008) (Appendix A4-B1).

As mentioned in section 2, the interior of Shackleton crater is a PSR (see Appendix A4-B4), and several others are located in the region. In addition to PSRs, 'cold traps' (Watson et al., 1961), are widely distributed within the South Pole region (see Appendices A4-B5 and A4-B6). These provide ideal locations for addressing NRC (2007) Concept 4 which broadly aims to investigate volatile flux throughout the history of the Solar System. It can be seen from Appendices A4-B5 and A4-B6 that in addition to Shackleton crater, neighboring craters Faustini, Shoemaker, and Haworth also contain cold traps of interest for ISRU purposes and are also worthwhile targets for exploration. Faustini crater is the only neighboring crater able to be investigated in this work due to the capabilities of the LER (Section 3.2). Elphic et al. (2007) documented an increasing hydrogen gradient across the floor of Faustini crater with a north/south orientation. The presence of this gradient makes Faustini a prime location for sample collection and measurement of volatile concentration and depth relative to surface temperature. The walls of Faustini crater also provide an ideal location for sampling of material subject to a temperature change gradient as they are steep, yet accessible given the parameters for this study.

Traverses and sampling stations for this landing site (Figure 15) are planned based on three main parameters: geologic unit (Spudis et al., 2008) (Appendix A4-B7), accessibility(slope) and volatile stability. Volatile maps used for this study are H_2O and CO_2 ice stability maps calculated from the temperature data from LROs Diviner Lunar Radiometer Experiment (Paige et al., 2010) (see Appendices A4-B5 and A4-B6).

NRC (2007) concepts addressed by the South Pole/Shackleton crater traverses are 1, 2, 3, 4, 6, and 7. For detailed station information, sample collection methods, sample types, and masses, as well as NRC concepts and goals addressed with this traverse please refer to the tabular breakdown in Appendix A2-B and Appendix A5-B.

Traverse Loop 1. Traverse 1 circumnavigates Shoemaker crater in an anti-clockwise direction, stopping to sample the hydrogen gradient across the floor of Faustini crater (Elphic et al., 2007), before continuing north to high priority Stations 8, 9, and 10 where extremely cold volatile rich regolith will be collected to address NRC (2007) Concept 4. LRO-LAMP (Lyman Alpha Mapping Project) data has detected geologically young impact crater in Faustini crater (Mandt et al., 2016) near Station 6, which could have excavated volatile-rich regolith directly to the surface and, thus, this station has a high priority. Station 11 is positioned between Haworth and Shoemaker craters, and is the only station in this traverse which is not located in a PSR (in order to robustly address NRC (2007) Concept 4 samples are needed from a large number of volatile rich locations). However, its position renders it suitable for obtaining imagery of both craters which will aid in the understanding of their stratigraphy and the vertical and lateral extent of volatiles in both Haworth and Shoemaker craters.

Traverse 1 is approximately 324 km long, taking a total of 12 days (77.7 hours) to complete with the inclusion of 11 EVA stations. It has an average slope 6.3°, and a maximum slope of 23.4°, see Appendix A4-B2.

Traverse Loop 2. Traverse 2, which circumnavigates de Gerlache crater in an anti-clockwise direction, contains sample stations located on four geologic terrains (pre-Nectarian terra material, Imbrian plains material, Orientale basin secondary crater material, and Eratosthenian crater material) (see Appendix A4-B7). Station 15 in particular is located on the contact between pre-Nectarian terra material and Imbrian plains material, and samples collected from this station can be used for further characterization of these two units which can address NRC (2007) Concepts 1, 4, 6, and 7 (see Appendix A4-B8).

Traverse 2 is approximately 320 km long, taking approximately 11 days (71.5 hours) to complete with the inclusion of 7 EVA stations. It has an average slope of 5.5°, and a maximum slope of 23.2°, see Appendix A4-B3. Similar to Traverse 1, this traverse explores locations within PSRs to maximize the collection of volatile rich regolith.

5.2.3. Schrödinger basin

Post-basin formation volcanism has resulted in the deposition of both mare basalts in the northern part of the smooth inner-peak ring floor of Schrödinger basin, and pyroclastic material emanating from a vent close

to the center of the basin (see Appendix A4-C1). Such materials are not only significant for their insight into lunar magmatism, but also for potential in-situ resource utilization (ISRU) applications. The identification of permanently shadowed regions (PSRs) within the basin (see Appendix A4-C1) indicate that volatile species may be present and stable on geological timescales. From the basin walls, it may be possible to sample the SPA basin impact melt sheet (Hurwitz and Kring, 2015).

Schrödinger basin has been well studied, with O'Sullivan et al. (2011) proposing three landing sites for human missions to its interior which focus on mare basalt deposits, the pyroclastic vent, the peak ring, impact melt breccia, or the Schrödinger melt sheet. Each site was constrained by a 10 or 20 km 'walkback' radius for the crew. Bunte et al. (2011) proposed a crewed sortie-reconnaissance mission in which a single landing site was located within the pyroclastic deposit, allowing access to the basin's inner ring and volcanic vent. Potts et al. (2015) designed two traverse routes for a 14-day solar-powered robotic mission to Schrödinger basin, while Steenstra et al. (2016) designed two traverses (a long and short route) based on a 3-year mission plan in support of the HERACLES mission concept (Landgraf et al., 2015). We incorporate all sampling locations from Steenstra et al. (2016) into this work.

In this traverse, we demonstrate the scientific gain from the longer duration, 42-day mission framework specified in the 2018 GER (International Space Exploration Coordination Group, 2018). We provide three traverse options, all of which can be utilized if crew-LER operations are permitted at night, or two of which can be utilized if crew need to remain at the landing site during lunar night.

The diverse geological terrains inside the basin, as seen in Figure 17, allow all seven NRC (2007) concepts to be addressed (Appendix A5-C). A detailed explanation of how these National Research Council (2007) concepts and goals are addressed by the traverses in the following sections is found in Appendix A2-C.

If the interior of Schrödinger basin cannot be accessed via the identified access point by the LERs due to slope constraints (Section 6, and Fig. 8), the crew would instead need to land outside of the basin. Such an exterior site would be limited in terms of geological context and notable features. In the external landing site we propose in Fig. 18, there is no access to young mare, pyroclastics, or feldspathic primary crust. External impact melts would also lack geological context, as the region is characterized by

rough terrain dominated by the products of other impacts. We recommend detailed slope studies be performed on finer resolution LROC NAC DEMs (1 m/pixel) to ensure access to the interior landing site is possible.

Traverse Loop 1. Traverse 1 travels broadly north of the landing site, passing through five different units as defined by Kramer et al. (2013) see Appendix A4-C1). The landing site is situated in the pyroclastic unit, and the traverse closely follows the 'short traverse' designed by Steenstra et al. (2016) which highlights the eastern peak ring as of particular interest, due to extensive M^3 data availability and its close proximity to the pyroclastic vent (Bunte et al., 2011; O'Sullivan et al., 2011; Potts et al., 2015). The identification of boulders and associated trails in the Steenstra et al. (2016) mission enable the collection of peak ring material from locations that are accessible using the LERs in this study.

Traverse 1 samples the base of the peak ring formation (Stations 1, 2, 3, and 4 addressing NRC (2007) Concepts 1, 2, 3, and 6) as well as the pyroclastic unit (Stations 5, 6, 7, 8, addressing NRC (2007) Concepts 1, 2, 3, 4, 5, and 7) before crossing the mare unit. At Station 13, the traverse samples a PSR at a crater within the smooth inner peak ring impact melt unit of the basin, which may act as a cold trap where volatiles are incorporated into regolith (Kring et al., 2014). Station 16 samples the FeO-rich ridge described by both Shoemaker et al. (1994) and Kramer et al. (2013), which is thought to be the result of either buckling of the melt sheet or later extrusion. Samples from this ridge may address NRC (2007) Concepts 1, 5, and 7.

Traverse 1 is approximately 267 km long, taking a total of 12.5 days to complete with the inclusion of 16 EVA stations. It has an average slope of 3°, and a maximum slope of 14.8° (Appendix A4-C4). Soil trafficability studies have previously been carried out by Steenstra et al. (2016) and indicate that the pyroclastic terrain is amenable to traverse by an LER. Traverse 1 is intended to take part in lunar day time, thus illumination is not a limiting factor to the activities planned.

Traverse Loop 2. Traverse 2 travels south of the landing site, passing through six different units as defined by Kramer et al. (2013) (see Appendix A4-C1). Beginning from the landing site in the pyroclastic unit, the traverse closely follows the southern portion of the 'long traverse' designed by Steenstra et al. (2016) that draws on previous studies (Bunte et al., 2011; O'Sullivan et al., 2011; Potts et al., 2015). Eight stations are included, at which boulders

from the peak ring, regolith from a secondary crater field, and impact melt breccias from the smooth and hummocky basin floor units are sampled.

Traverse 2 is approximately 205 km long, taking a total of 9.5 days (49 hours) to complete with the inclusion of 8 EVA stations. It has an average slope 2°, and a maximum slope of 9.7° (Appendix A4-C5).

Traverse Loop 3. After returning to the landing site to restock the LERs, crew travel farther south of Traverse 2 to explore the southern-most part of Schrödinger basin. Traverse 3 passes through six different units as defined by Kramer et al. (2013) (see Appendix A4-C1), continuing along the 'long traverse' designed by Steenstra et al. (2016) that draws on previous studies (Bunte et al., 2011; O'Sullivan et al., 2011; Potts et al., 2015). Ten stations are included, sampling boulders from the peak ring, regolith from a secondary crater field, and impact melt breccias from the smooth and hummocky basin floor units. Slope maps and NAC imagery have been used to plan traverses within engineering constraints of the mission, however a thorough study of the trafficability of LERs along collapsed material at the base of the wall and along terraced material must be conducted in the future.

In the absence of additional studies concerning the feasibility of operations during lunar night, this traverse has been planned such that lunar daytime will begin as the crew approaches the first sampling station (Station 25), see Appendix A4-C2. Lighting conditions during this part of the mission are crucial as the crew will be observing the terrain changes and imaging the stratigraphy of the terraced zone. Stations in this traverse are closely spaced, collecting rakes, scoops and impact melt breccias from the wall material and smooth hummocky floor units.

Traverse 3 is approximately 284 km long, taking a total of 12.5 days to complete with the inclusion of 10 EVA stations. It has an average slope of 5.9°, and a maximum slope of 19.7° (Appendix A4-C6).

5.2.4. Antoniadi Crater

At Antoniadi crater we find that the presence of both a peak-ring and a central peak structure may provide the opportunity to sample material uplifted from the lunar crust, as well as the SPA impact melt sheet, which could be compared to similar samples from Schrödinger basin to address NRC (2007) Concept 6.

Antoniadi crater contains nine geologic terrains mapped by Sruthi and Kumar (2014) (see Appendix A4-D1A), who also identified and classified

45 volcanic cones based on circular topography and the presence of central pits, using spectral data to refine their composition (Fig. 19). Samples from these cones may also provide insight into lunar magmatic processes as pyroclastic material may be accessible, and would provide ground truth for imaging spectroscopy analyzes. Also noteworthy is the mare basalt in Antoniadi crater which is thought to be some of the youngest on the farside of the Moon (Wilhelms et al., 1979; Pasckert et al., 2018). This may also be compositionally different from the nearside/equatorial mare basalts that have been sampled previously (Pasckert et al., 2018). Recent crater counts suggest an age of 1.6 Ga for the unit around the central peak and 2.6 Ga for the outer floor unit near the basin wall (Haruyama et al., 2009; Sruthi and Kumar, 2014). These divergent ages suggest episodic volcanism has occurred in the crater. Due to the wide range of geologic units within Antoniadi crater, we submit that all NRC (2007) concepts may be addressed at this site (see Appendix A2-D and Appendix A5-D).

The exploration zone and related scientific goals are based on previous work by Clark et al. (2009), Fagan et al. (2010), and particularly Sruthi and Kumar (2014) as they have produced the most detailed and current geologic map of the basin.

If the interior of Antoniadi crater cannot be accessed via the identified access point by the LERs due to slope constraints (Fig. 10), the crew would instead need to land outside of the crater. Such an exterior site would be limited in terms of geological context and notable features. In the external landing site we propose in Figure 20, there is no access to young mare, or feldspathic primary crust. External impact melts would also lack geological context, as the region is characterized by terrain dominated by the products of other impacts.

Traverse Loop 1. Traverse 1 explores the northern portion of Antoniadi crater, as shown in Figure 19. The traverse passes through or along six geologic units as mapped by Sruthi and Kumar (2014). These units are: central peak, peak ring, hummocky floor, smooth floor, wall material, and mare basalt (see Appendix A4-D1A). A total of 16 stations are dispersed throughout these units as well as along key contact points to maximize and diversify sampling.

Traverse 1 is approximately 253 km long, taking a total of 12 days (90 hours) to complete with the inclusion of 16 EVA stations. It has an average slope of 2.6°, and a maximum slope of 13.2° (Appendix A4-D2). If crew-LER

operations are permitted during lunar night, this traverse has been designed to be conducted during this time as illuminated conditions are more essential for Traverse 2, in which photography of the crater wall has been planned.

Traverse Loop 2. Traverse 2 explores the southern portion of Antoniadi crater as illustrated in Figure 19. This 395 km traverse passes through or along seven geologic units as mapped by Sruthi and Kumar (2014). These units are young crater ejecta, peak ring, hummocky floor, smooth floor, impact melt, wall material, and mare basalt (see Appendix A4-D1A). A total of seven stations are dispersed throughout these units as well as along key contact points to maximize and diversify sampling.

Along the traverse from stations 20 through 23, documentation of the crater wall will be conducted via Gigapan imagery, addressing NRC Concepts 1, 2, 3, and 6. Whilst slope maps and NAC imagery indicate that traversing along the crater wall and through portions of terraced material is feasible, a thorough study of the trafficability of LERs along the collapsed material at base of the wall and along the terraced material needs to be conducted.

As this traverse is largely conducted along the basin wall, it is crucial that this traverse be conducted during the sunlit period of the lunar day to allow for photography of stratification within the wall material as well as ensuring a safe traverse for crew over potentially rough terrain.

Along this traverse, there is an average slope of 3.5° with a maximum slope of 14.3° (Appendix A4-D3). The total traverse time is 13 days (98 hours), including a total driving time of 79 hours, 7 EVA stations, communication dropout, and landing site breakdown operations.

5.2.5. South Pole–Aitken Basin Center

Traverses planned for this site can be seen in Figure 21. As mentioned in section 2 despite its age the basin still maintains a distinctive FeO chemical signature (Gibson and Jolliff, 2011; Moriarty and Pieters, 2018). This compositional anomaly extends across the flat interior floor of the basin related to both volcanic and non-volcanic materials and is likely composed of impact-melt breccia leftover from the extreme event that created the basin. If able to be sampled, these impact-melts can be used to refine the age of the basin and address NRC (2007) Concepts 1 and 6.

Nearby the landing site are mare and cryptomare deposits mapped by Borst et al. (2012) and Gibson and Jolliff (2011) with conflicting extents. These volcanic materials would help to resolve these discrepancies and may

address NRC (2007) Concepts 2, 3, and 5. Additionally, as mare basalts on the nearside range from 4.2 - 1.2 Ga, sampling from across the SPA basin would determine if farside volcanism shares a similar timeline (Jaumann et al., 2012; Pasckert et al., 2018).

To the northwest of the landing site is Bose crater which is approximately 90 km in diameter and contains a central peak (of diameter 15 km) and a terraced crater wall. This central peak and crater wall (along with that of Bhabha crater) exhibit low-calcium pyroxene noritic composition, which is though to represent thick impact melt breccia associated with the SPA-basin forming impact. No other regions of noritic composition have been identified, suggesting that the norite was uplifted by the rebound during the impact. Overlaying this noritic material is a gabbroic layer (Borst et al., 2012) which may represent the remnants of the differentiated mafic SPA impact melt sheet (Pieters et al., 2001). Sampling of this layer may address NRC (2007) Concept 6.

Furthermore, areas within the SPA basin have received some of the lowest contributions of non-SPA derived material, between 20–50% of both impact-melt and foreign materials (Petro and Pieters, 2004; Petro and Jolliff, 2011). Thus, samples of ancient regolith at this location will be less contaminated by non-SPA materials and address Concept 7.

The Mars-forward 100 km exploration zone within the SPA basin center involves investigation of the Mafic mound, Bose and Bhabha craters, a small, unnamed geologically young crater, mare and cryptomare deposits, and ancient regolith deposits (Fig. 21).

The region contains 7 geologic terrains from pre-Nectarian to Imbrian age (Wilhelms et al., 1979). Borst et al. (2012) defined 9 geologic units for the study region, however, the mare/cryptomare boundaries are disputable when compared to those of Gibson and Jolliff (2011) (see Appendices A4-E1, A4-E2, A4-E3). Traversing in this region will help to address these discrepancies and comparison of samples from multiple adjacent flows would provide temporal and compositional context for volcanism in the SPA basin center.

The diverse set of lithologies within the proposed portion of the SPA basin center allows for NRC (2007) Concepts 1, 2, 3, 5, 6, and 7 to be addressed (Appendix A5-E). A detailed explanation of the specific NRC goals that can be addressed by the traverses in the following sections can be found in Appendix A2-E.

Traverse Loop 1. The first traverse travels broadly south, visiting the Mafic mound (Moriarty and Pieters, 2015). To investigate its origins we plan numerous opportunities to sample putative impact melt of the SPA basin forming event (Stations 4-7) and address Concept 1 to test the lunar cataclysm hypothesis. Furthermore, the ejecta blanket of Bhabha crater (Stations 1-3) can determine the age of the subsequent impact event, and ancient regolith collected from various locations (Stations 4-7, 9) can investigate the nature of regolith processes in the SPA basin center and address Concept 7. Additionally, cryptomare deposits (Stations 7-9, 11) can be sampled to address Concepts 2, 3 and 5 to reveal the nature of the lunar farside volcanism.

Traverse 1 is approximately 308 km in length, taking a total of 13 days (97 hours) to complete with the inclusion of 11 EVA stations and a 1.6 day pause due to orbital communication loss. It has an average slope of 3.6° and a maximum slope of 14.7° (Appendices A4-E4, A4-E5).

Traverse Loop 2. The second traverse circumnavigates north and explores the central peak (Station 14), crater wall (Stations 12, 15) and impact melt (Station 13) of Bose crater, sampling ancient regolith (Stations 12, 13, 15), as well as mare (Station 16) and cryptomare deposits (Stations 17, 18) (see Appendices A4-E2 and A3-E3).

The impact melt pond of Bose crater can be used to accurately determine the age of crater-forming impact. Additionally, collecting samples of impact melt from a number of locations may provide insight on the nature of lunar history and chronology. Sampling of the central peak of Bose crater may provide crucial information as to the presence, composition and possible differentiation of the SPA melt sheet. SPA impact melt sheet may be accessible from crater wall exposures, thus sampling stations have also been selected to sample wall material. Traverse 2 is approximately 360 km long, taking a total of 14 days (103 hours) to complete with the inclusion of 7 EVA stations. It has an average slope 3.2°, and a maximum slope of 6.1° (Appendices A4-E4, A4-E6). We recommend this traverse take place in the lunar daytime due to the terrain variation when descending into Bose crater.

6. Implied Trade Studies

This study revealed several shortcomings in existing data and analysis. As such, we suggest that the following issues need more attention.

Detailed illumination studies were not possible for these sites due to the limited resolution of DEMs available in the edition of the Lunar Mapping and

Modelling Project (LMMP) available at the time of the study. Thus, a future trade study must be conducted for all sites at a high resolution, especially along traverses where the LER is limited to daylight driving only to maximize hazard avoidance, increase visibility for crew and maximize scientific return from Gigapan deployment.

Also with respect to illumination, we assume the LERs are able to drive through PSRs, but the maximum duration of transit in darkness is not yet constrained and requires an additional trade study. Detailed illumination data should be collected and investigated in multiple dimensions (to determine if the entire LER will be in shadow, or partially in shadow) in order to assess thermal load on the LER and partially address the allowable time and distance it may travel in a PSR. Studies concerning the power source type, availability of solar power, and/or rechargability of the LERs are also required in order to factor in recharge times for all traverses.

Additionally, without accurate estimations of the reduced productivity of the astronauts and the LERs during lunar darkness, this study assumes the same rate of both IVA and EVA ability. Thus, there is a need for a trade study which investigates both driving and sampling in limited illumination conditions. Also, visual and experimental time requirements are necessary for different instruments on board the LER(s) utilized along the scientific traverse between sites.

If an autonomous mode were considered for the LERs over terrain that had already been well-characterized, whether already traversed, characterized from high-resolution orbital imagery, or from Gigapan imagery taken along the traverse, LER speed would have to be slowed in order to minimize risk to the vehicles. This would have the follow-on effect of increasing traverse time, however, as long as this remains within the 30% contingency margin allotted to the 1-year travel time between landing sites then such a mode could be considered. Autonomy, or partial-autonomy, may also be particularly useful when considering prospecting operations, or continuous sub-surface surveys over well-characterized regions. We recommend a future trade study be performed concerning the feasibility (time loss, risk minimization, hazard detection and avoidance) of autonomous navigation.

Future trafficability studies may be required to access to Schrödinger basin and Antoniadi crater in greater detail. This may involve the creation of high resolution NAC DEMs in order to facilitate hazard avoidance while the LER are tele-operated and elucidate the effect of poorly consolidated material on their access to human landing sites. Furthermore, additional hazard

studies, such as rock abundance and crater density between, in, and around landing sites are necessary for more detailed traverse planning because 0.5 to 1.0 m resolution NAC imagery was not available along the entire routes we investigated.

Alternative traverse routes should be planned in the event that LER slope capabilities change in the future. This may be done parametrically, cycling through potential slope values in steps (e.g. 15, 20, 25, 30 degrees) and assessing how this affects the science able to be obtained from these alternate routes. Another angle to such a study would be to plan alternate traverse routes depending on the chosen orbital configuration – assessing how travel times, communications, and science gains will change if a Near-Rectilinear Halo Orbit is selected.

In terms of future LOP-G studies, a study to optimize LOP-G visibility by using its capability to change its orbital phase, and demonstrate its propulsion system, would be valuable. Additionally, detailed studies of LOP-G visibility from the lunar surface taking into account the occultation of the LOP-G by local terrain may be of interest.

In terms of additional data requirements, to maximize the scientific return detailed geologic maps of the South Pole (Malapert massif and Shackleton crater area) and South Pole-Aitken basin center would be required. While spectroscopic data is limited at such high latitudes, future studies may also wish to concentrate on the collection of this valuable data in order to further refine material composition for sample collection.

While our analyzes provide minimum mass estimates based on the assumption of rock and soil as the sampled material, volatile-rich and icy material should also be taken into account. It appears the landing sites and traverses will potentially provide access to them as well. Research into the transport and storage of volatile-containing samples must also be undertaken to ensure no sample context is lost upon transport back to Earth.

For this study, while 'safe' distances were calculated for traverses between landing sites, and a 100 km exploration radius was used for planning traverses at and around landing sites, in reality, traverses will be much shorter to take into account a variety of additional contingencies that arise from further detailed mission planning. In the course of this study we did undertake preliminary crew activity planning in order to estimate overall traverse timing which is not discussed in this paper; however, an example crew activity timeline for Schrödinger basin is included in Appendix A4-C2) to facilitate future research in this area.

We also suggest an investigation of notional instrument payloads (taking into account their dimensions, power consumption, and masses) which would maximise science return along the proposed traverses. For example, a visible to near-infrared (VNIR) multispectral camera or hyperspectral imaging spectrometer could aid in the ground-truthing of orbital data from Chandrayaan-1s M^3 instrument. A mass spectrometer like NASAs Sample Analysis at Mars (SAM) instrument (Mahaffy et al., 2012), or ESAs Package for Resource Observation and in-Situ Prospecting for Exploration, Commercial Exploitation and Transportation (PROSPECT) Sample Preparation and Analysis (ProSPA) instrument (Carpenter et al., 2014; Barber et al., 2017) may be included for volatile analyzes. A drill, whether carried as an instrument by crew on EVA, or attached to the LER as with ESAs ExoMars 2020 rover (Vago et al., 2017), could also be used to investigate the vertical distribution of subsurface material and collect well-preserved material for analysis. Using the hole created by the drill, the crew could deploy a heat-flux experiment package to measure heat flow coming from the interior of the Moon and address NRC Goal 2d – characterize the thermal state of the interior. The PrActive or passive seismometers could also be carried as part of the instrument payload. Deployment of these seismometers at each proposed landing site, effectively forming a seismometer array, could help to characterize the lunar crust, mantle, and core and address NRC Concept 2.

Additionally, in order to address the recent impact flux (NRC Goal 1d) at (and potentially between) all proposed landing sites a camera positioned onboard the LOP-G could provide regular surface monitoring which could be used to locate fresh craters for sampling by crew on subsequent missions, or for the LERs to remotely investigate between crew landings if they are equipped with a sample collection ability.

Manual estimation of regolith thickness could be performed for traverses in this region by examining the size and morphology of concentric craters using the method described by Oberbeck and Quaide (1968) and as performed by Huang et al. (2018) for the Chinese lunar mission Chang'E 4. These regolith thickness estimations could then be "ground truthed" during the proposed mission using GPR measurements between and at all landing sites.

Once the results of the above trade studies have been obtained, traverse and EVA times presented here may be calculated more accurately depending on the task and priority of each station, and whether it is scheduled to be visited in lunar daytime or nighttime.

7. Conclusions

This study, based upon a design reference mission by Hufenbach et al. (2015) as a prelude to the release of the 2018 GER, is a first-pass at the feasibility of a five-site, LOP-G enabled, lunar sample return mission scenario which utilizes both human and robotic assets. The findings of this study, obtained through integration of multiple remotely-sensed lunar datasets, robotic asset capabilities, and communications feasibility, show that a human-assisted robotic mission to the lunar south polar region, including farside locations, can address all seven NRC (2007) lunar science concepts, and would be a valuable resource for the early history and evolution of the Solar System.

The traverses between the five landing sites seem feasible within the known engineering capabilities of the LER(s). Our accessibility study identified possible access to the interior of Schrödinger basin and Antoniadi crater. Although, if future study of higher-resolution datasets, such as NAC DEMs, reveals that these basin floors are inaccessible, exploration zones must be limited to exterior surface locations, which would mean that significant geological context is lost (Figs. 18 and 20).

We find that tele-operating the LERs between the five proposed landing sites along 'science' traverses can enable a significant amount of science to be performed while remaining within the allotted travel time and slope requirements with 30% contingency. Distances between landing sites are sufficiently short (approx. 1000 km) and LER speed is sufficiently fast (0.36 km/hr) to conduct significant geological surveys during 'science' traverses, some of which involve prospecting for icy volatiles in Cabeus and Amundsen craters. We recommend the addition of sample collection technology, such as a robotic arm, to facilitate this.

Given current engineering parameters it is not possible for the crew to fully explore a 100 km exploration zone in 28-day or 42-day missions, however, they are able to collect samples that address all, or a large fraction of the NRC (2007) objectives, depending on the landing site. In the future using variable rover speeds and EVA times on different terrain types will increase the maximum possible traverse distance adhered to in this study.

To maintain consistent communication across all landing sites we have selected a large southern-class halo orbit with an orbital period of 10.6 days for the LOP-G, based on calculations performed by Lockheed Martin (2016).

As the parameters for such a mission are likely to change based on results from future trade studies and asset engineering, components of this study are

highly amenable to adaptation as necessary; similar assessments may be undertaken for any proposed landing site. We find that surface exploration and sample return from human-assisted robotic exploration of the lunar surface would allow the international community to progress in its vision for larger scale, Mars-forward campaigns and provide valuable insight for future lunar exploration activities.

Acknowledgments. This work was carried out through the 2016 Exploration Science Summer Intern Program hosted by the Lunar and Planetary Institute (LPI) and Johnson Space Center (JSC). This research was supported in part by the NASA Solar System Exploration Research Virtual Institute (SSERVI). Thank you to Josh Hopkins and Chelsea Welch at Lockheed Martin for their calculations of orbital coverage for the given landing sites, and the Lunar Mapping and Modeling Project (LMMP) support staff (now Moon Trek).

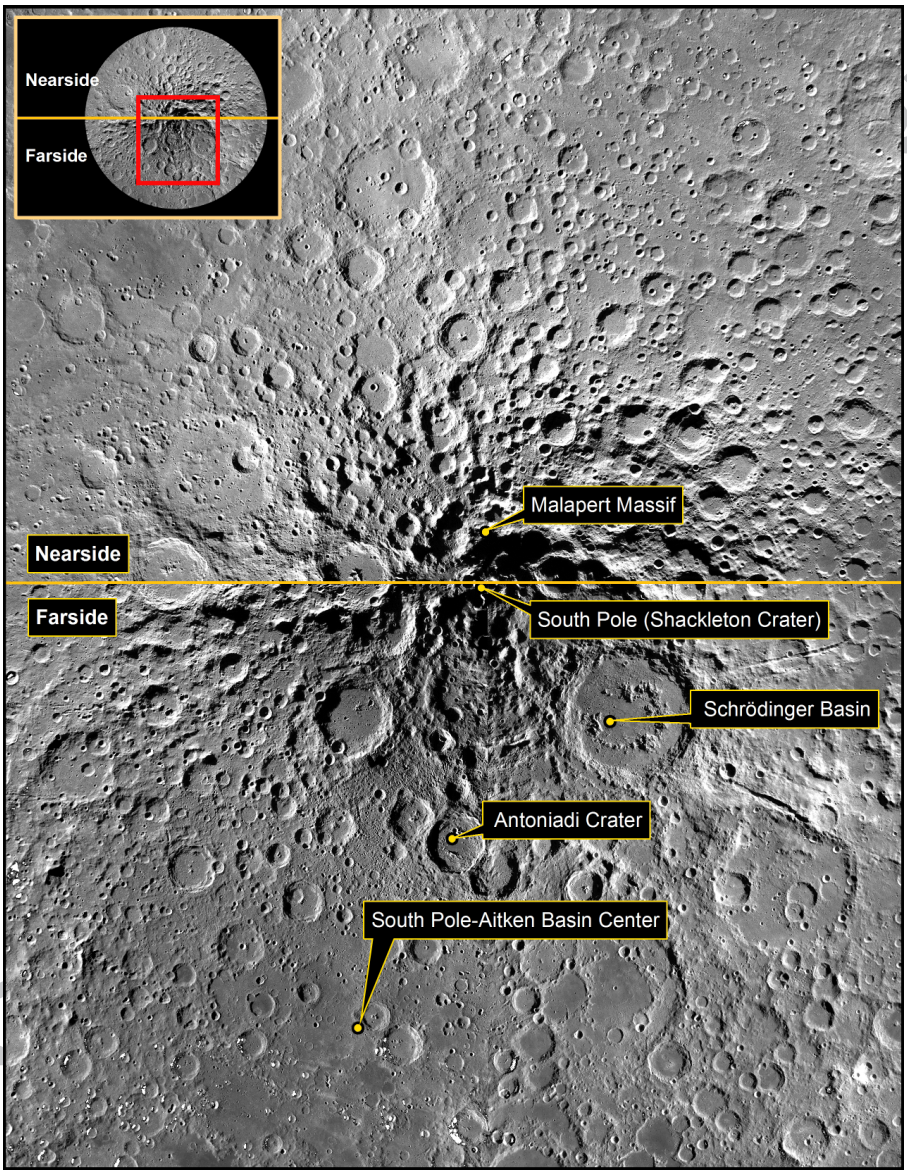

Figure 1: An overview of all landing sites considered in this study displayed on a LROC WAC mosaic of 100 m/pix. Projection is south polar stereographic.

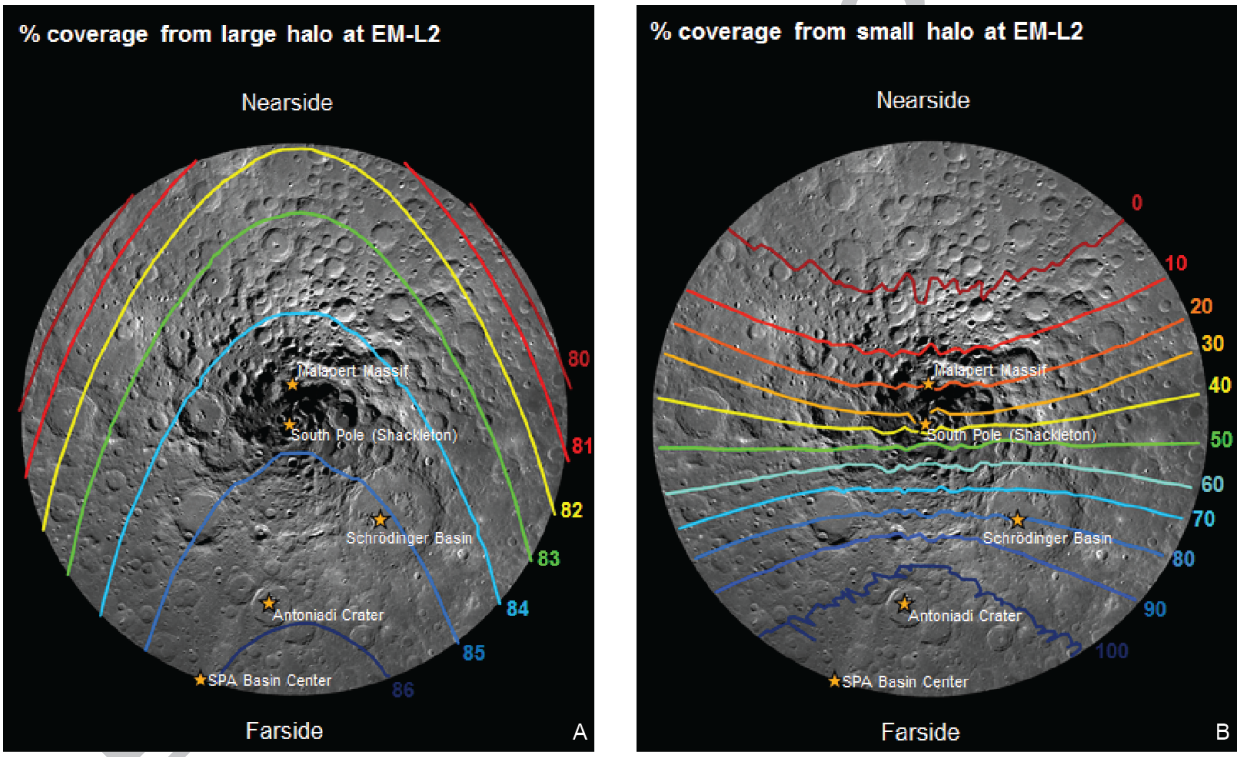

Figure 2: Percentage communication coverage for landing sites provided by large (A) and small (B) halo orbital configurations (Lockheed Martin, 2016).

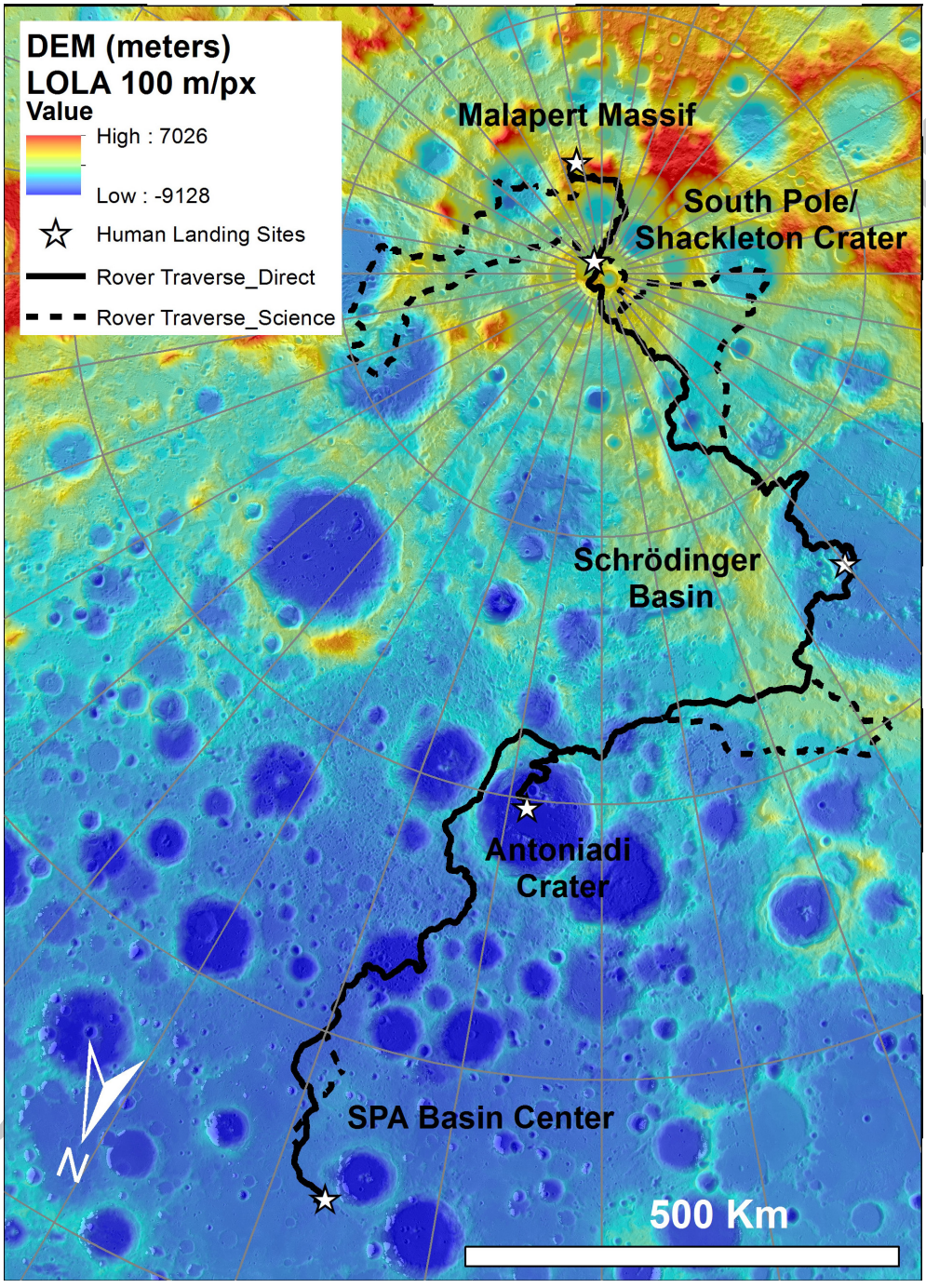

Figure 3: Colorized DEM of between landing site traverses from Malapert massif to South Pole-Aitken basin center displayed on a LRO LOLA mosaic of 100 m/pix. Direct traverse shown with a solid line, while science traverse shown with a dotted line and landing sites with white stars. North is towards every direction from the south pole shown by the grey polar stereographic grid. The traverses progress gradually north, as shown with an arrow in their direction.

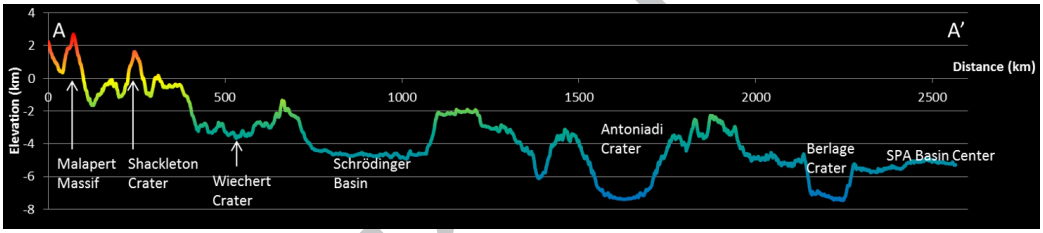

Figure 4: Colorized slope profile corresponding with the legend from Figure 3 of between landing site traverses from Malapert massif to South Pole-Aitken basin center. Note that the overall the route progresses downhill into the center of the basin.

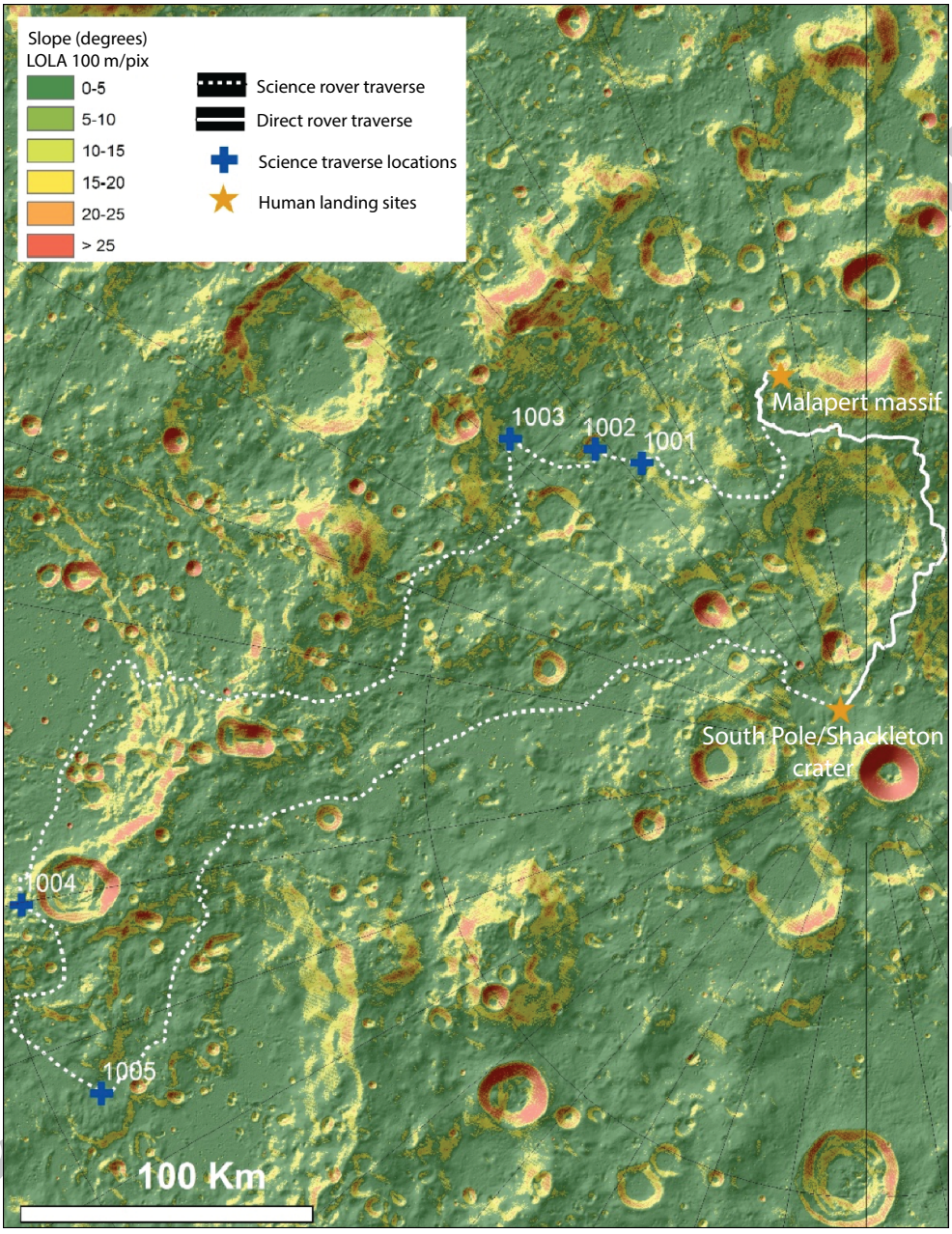

Figure 5: Direct and science traverses for Malapert massif to South Pole/Shackleton crater. Direct traverse shown with a solid line, while science traverse shown with a dotted line and stations of interest marked with blue crosses. The slope base map created from a LOLA 100 m/pix DEM overlaid on a LOLA hillshade. North is along every grid direction from the South Pole as shown by the polar stereographic projection.

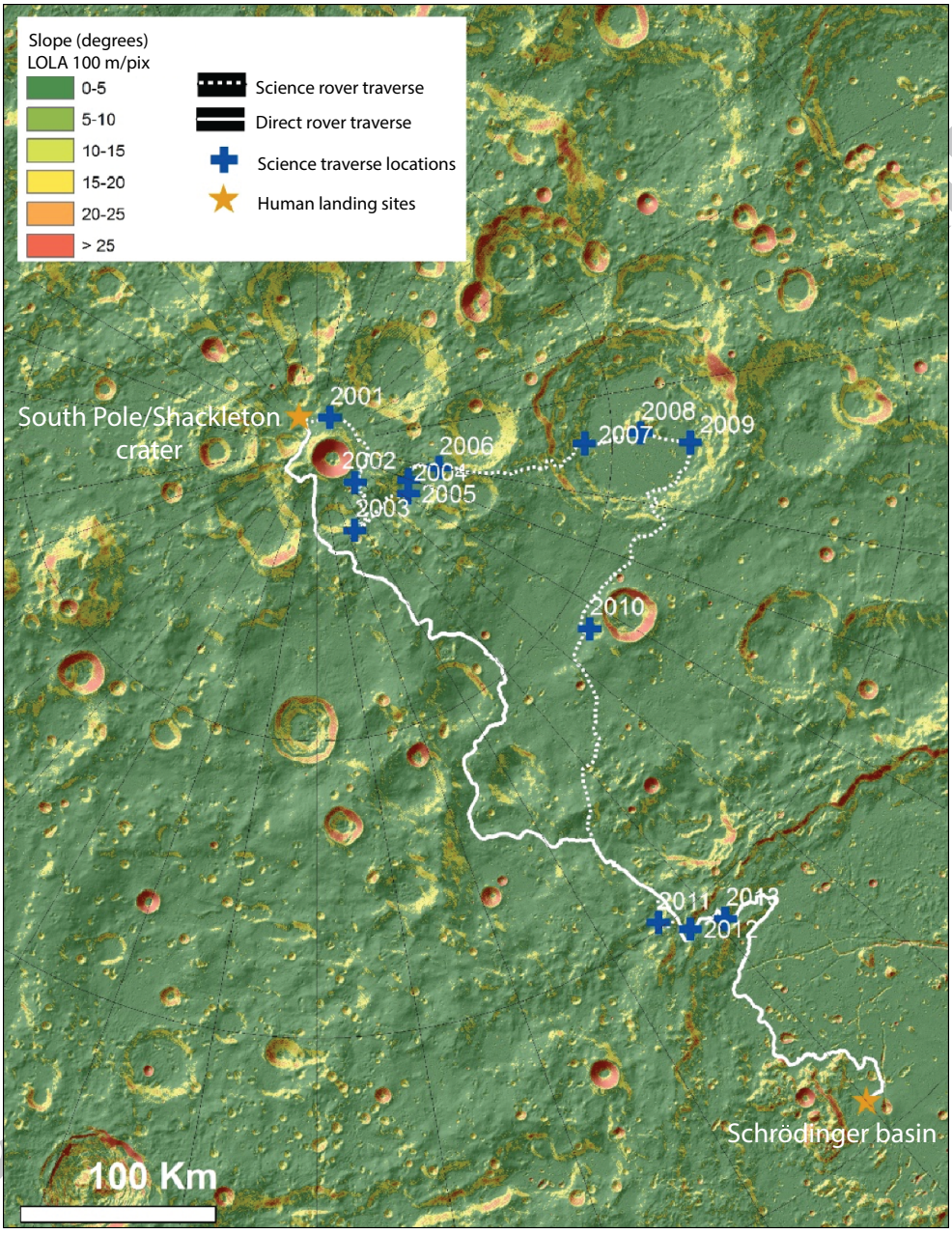

Figure 6: Direct and science traverses for South Pole/Shackleton crater to Schrödinger basin. Direct traverse shown with a solid line, while science traverse shown with a dotted line and stations of interest marked with blue crosses. The slope base map created from a LOLA 100 m/pix DEM overlaid on a LOLA hillshade. North is along every grid direction from the South Pole as shown by the polar stereographic projection.

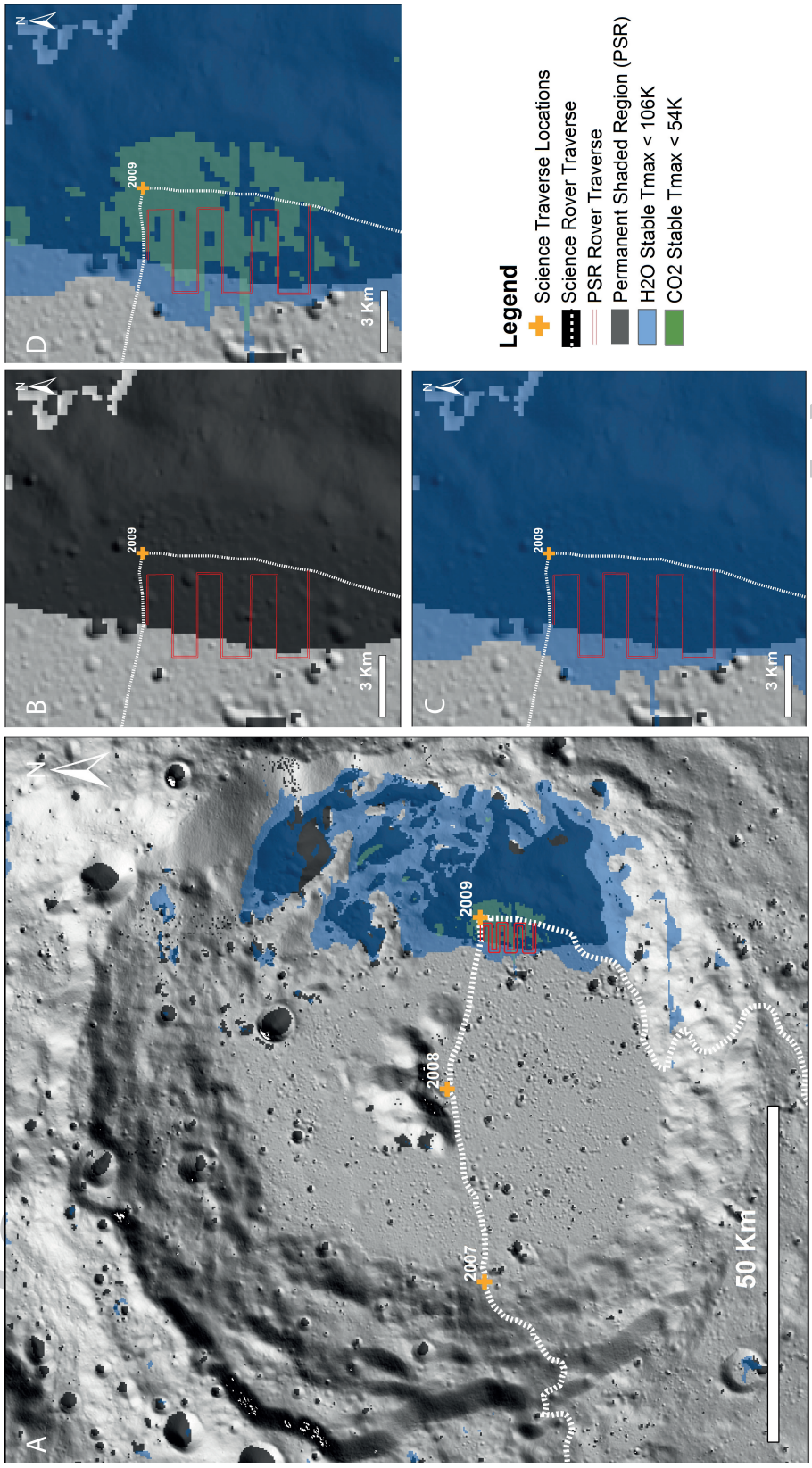

Figure 7: (A) The science traverse is shown descending to the interior of Amundsen crater. Stations of interest are marked in orange. (B) The path of the science traverse passing through a PSR, with an additional prospecting route shown in red. (C) Shows panel B route overlaid with a blue region in which H2O ice is stable (at temperatures < 106K). (D) Shows panel C additionally overlaid with regions in which CO2 ice is stable (at temperatures < 54 K). Prospecting though these regions would enable the lateral composition and distribution of lunar volatiles to be examined.

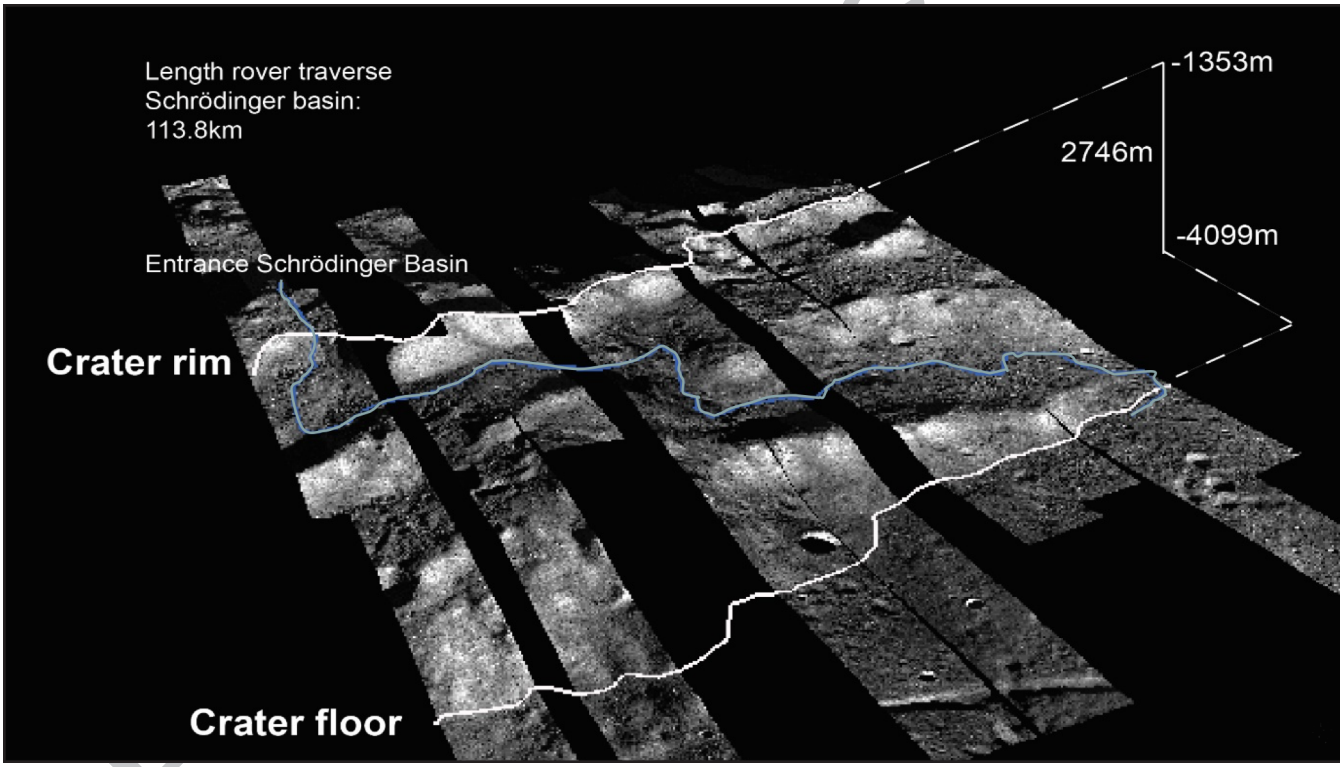

Figure 8: 3D image of Schrödinger basin wall. NAC mosaic draped over 60m resolution DEM. Blue line represents proposed rover traverse.

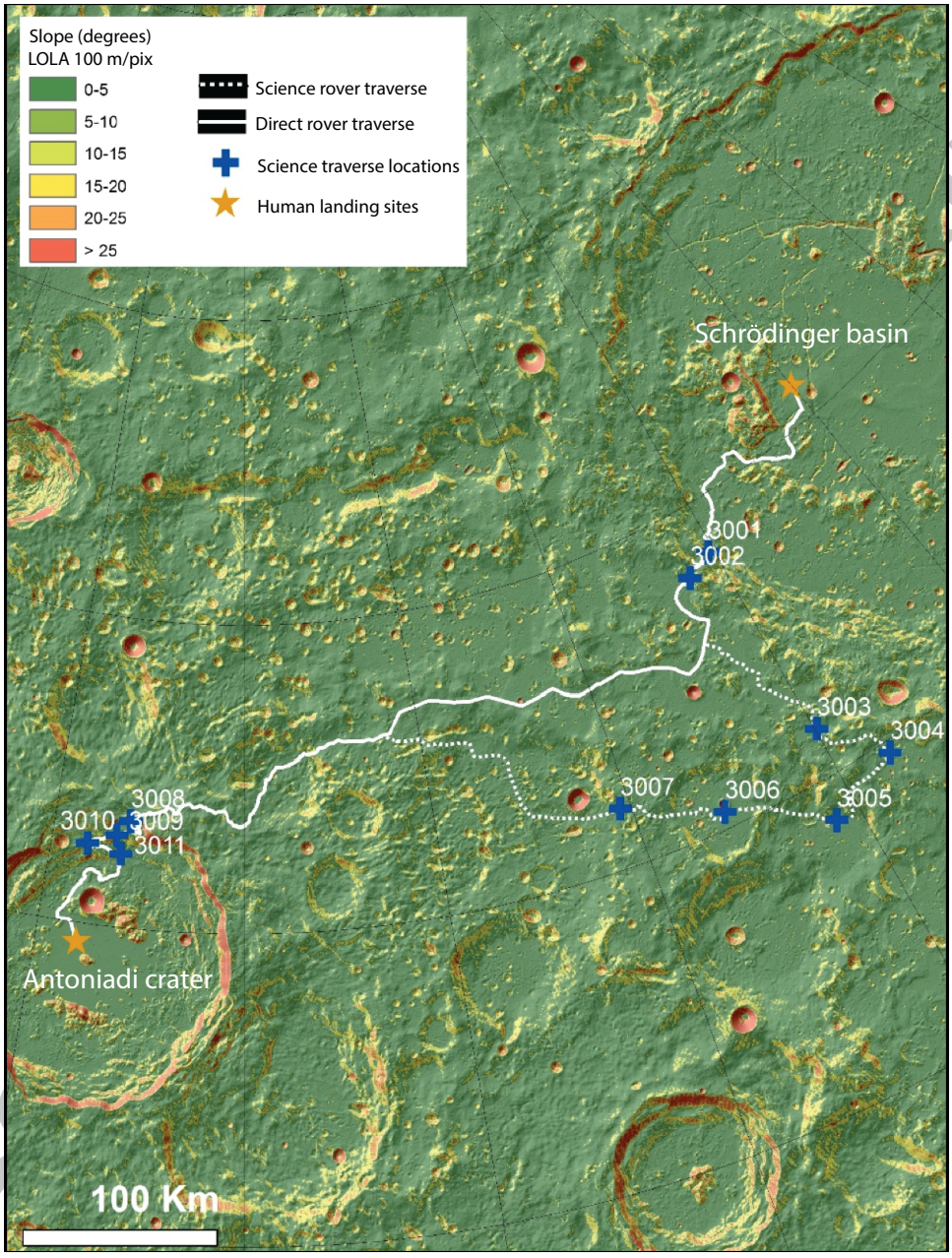

Figure 9: Direct and science traverses for Schrödinger basin to Antoniadi crater. Direct traverse shown with a solid line, while science traverse shown with a dotted line and stations of interest marked with blue crosses. The slope base map created from a LOLA 100 m/pix DEM overlaid on a LOLA hillshade. North is along every grid direction from the South Pole as shown by the polar stereographic projection.

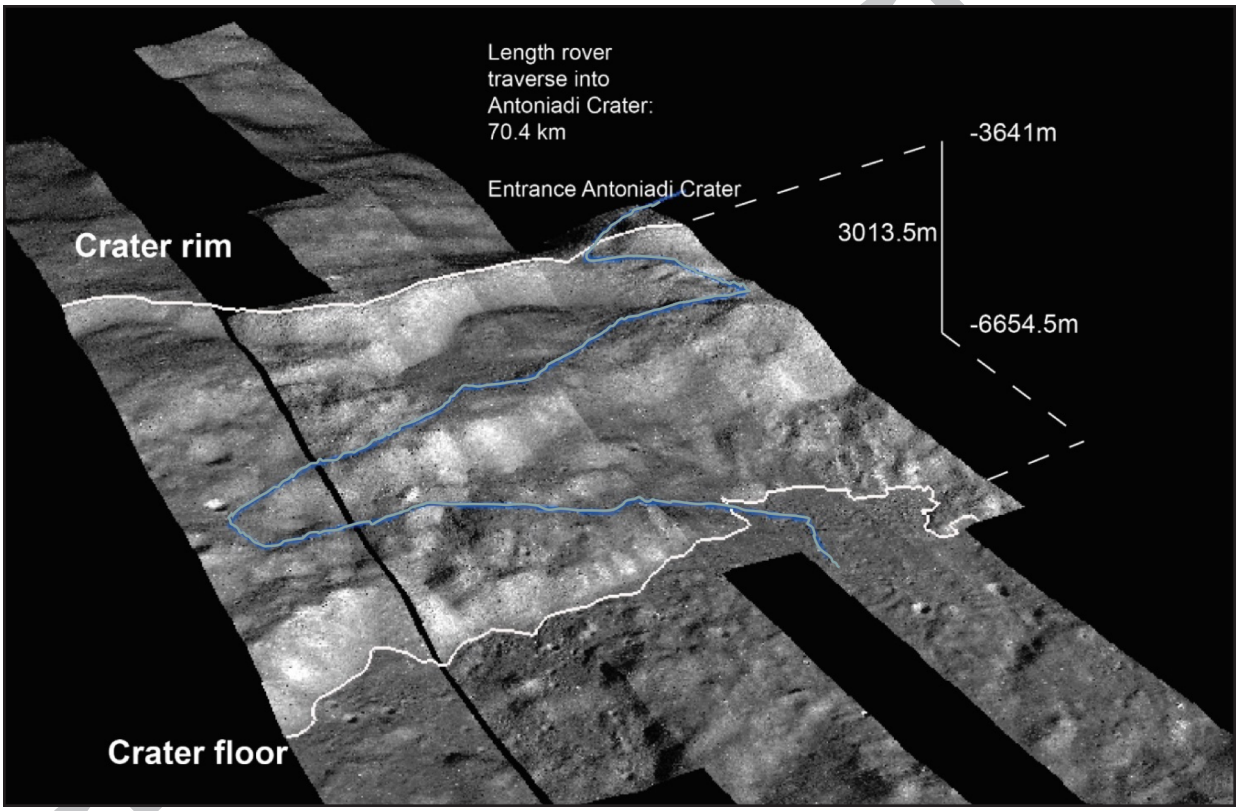

Figure 10: 3D image of Antoniadi crater wall. NAC mosaic draped over 60 m resolution DEM. Blue line represents proposed rover traverse.

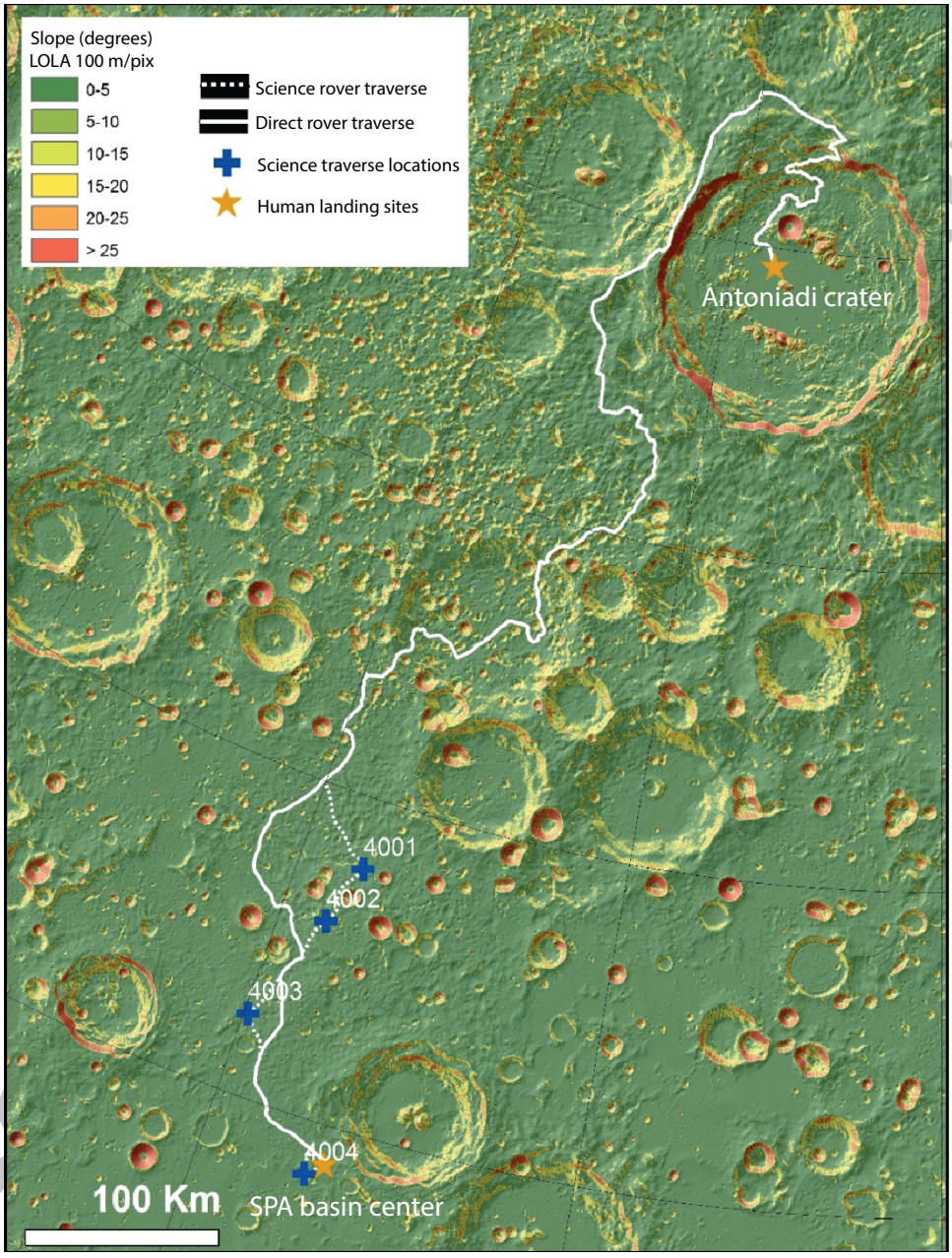

Figure 11: Direct and science traverses for Antoniadi crater to South Pole-Aitken basin center. Direct traverse shown with a solid line, while science traverse shown with a dotted line and stations of interest marked with blue crosses. The slope base map created from a LOLA 100 m/pix DEM overlaid on a LOLA hillshade. North is along every grid direction from the South Pole as shown by the polar stereographic projection.

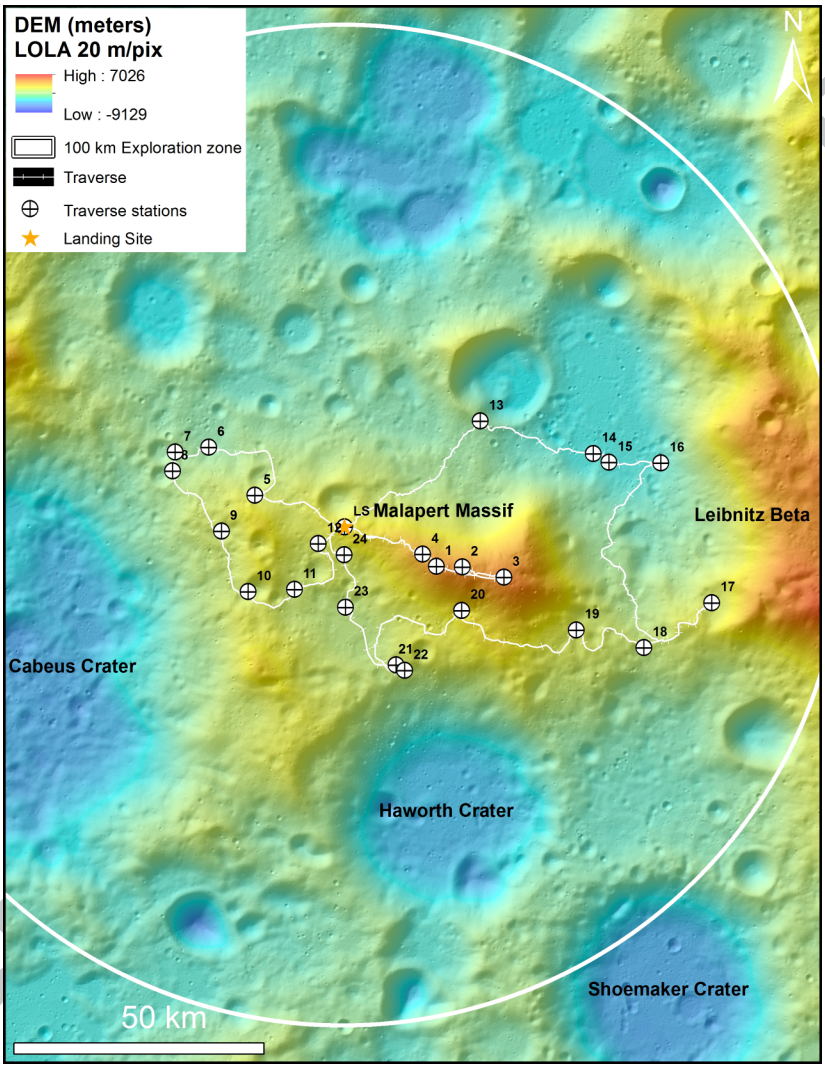

Figure 12: Colorized Lunar Orbiter Laser Altimeter (LOLA) Digital Elevation Model (DEM) of Malapert massif overlaid on an LROC WAC mosaic of 100 m/pix. Includes traverses, sampling stations, and 100 km Mars-forward exploration zone for reference.

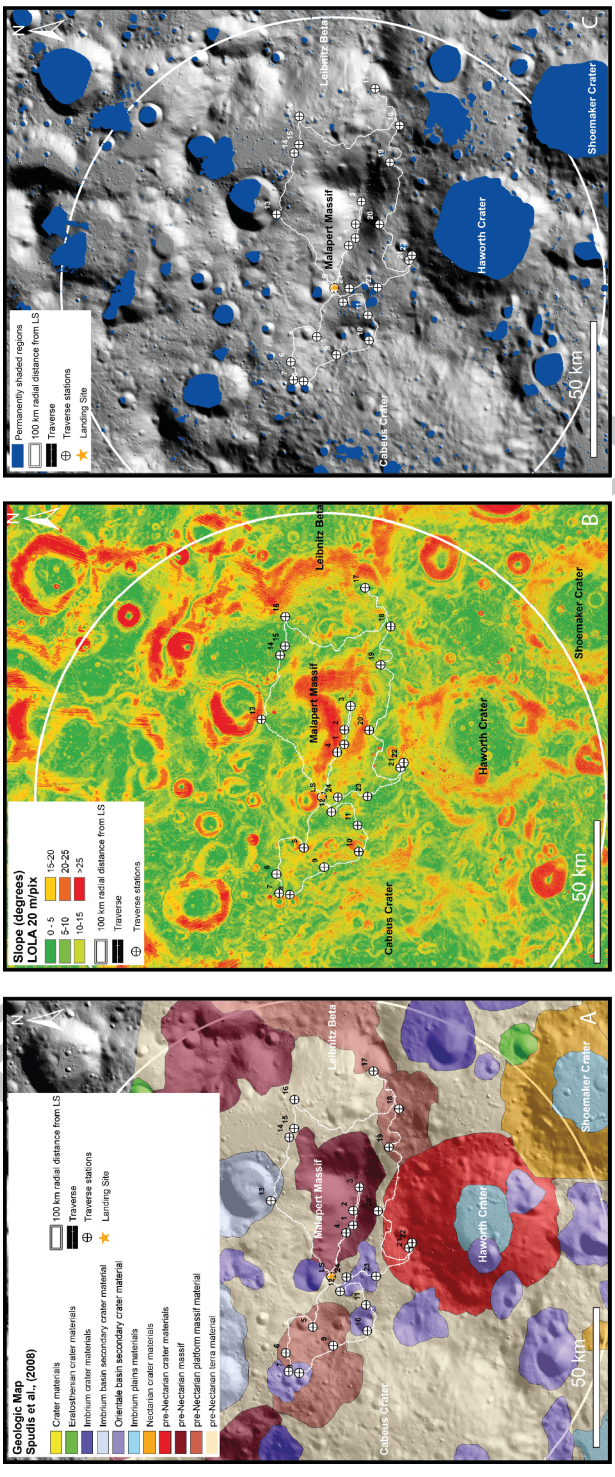

Figure 13: A: Spudis et al. (2008) map of geologic units combined with Malapert massif at-site traverse and a 20 m/pix hillshaded LOLA DEM. B: Slope map (20 m/pixel from LOLA DEM) combined with the Malapert massif at-site traverse. C: Locations of Permanently Shadowed Regions in the region of Malapert massif overlain on a LROC WAC 100 m/pix mosaic.

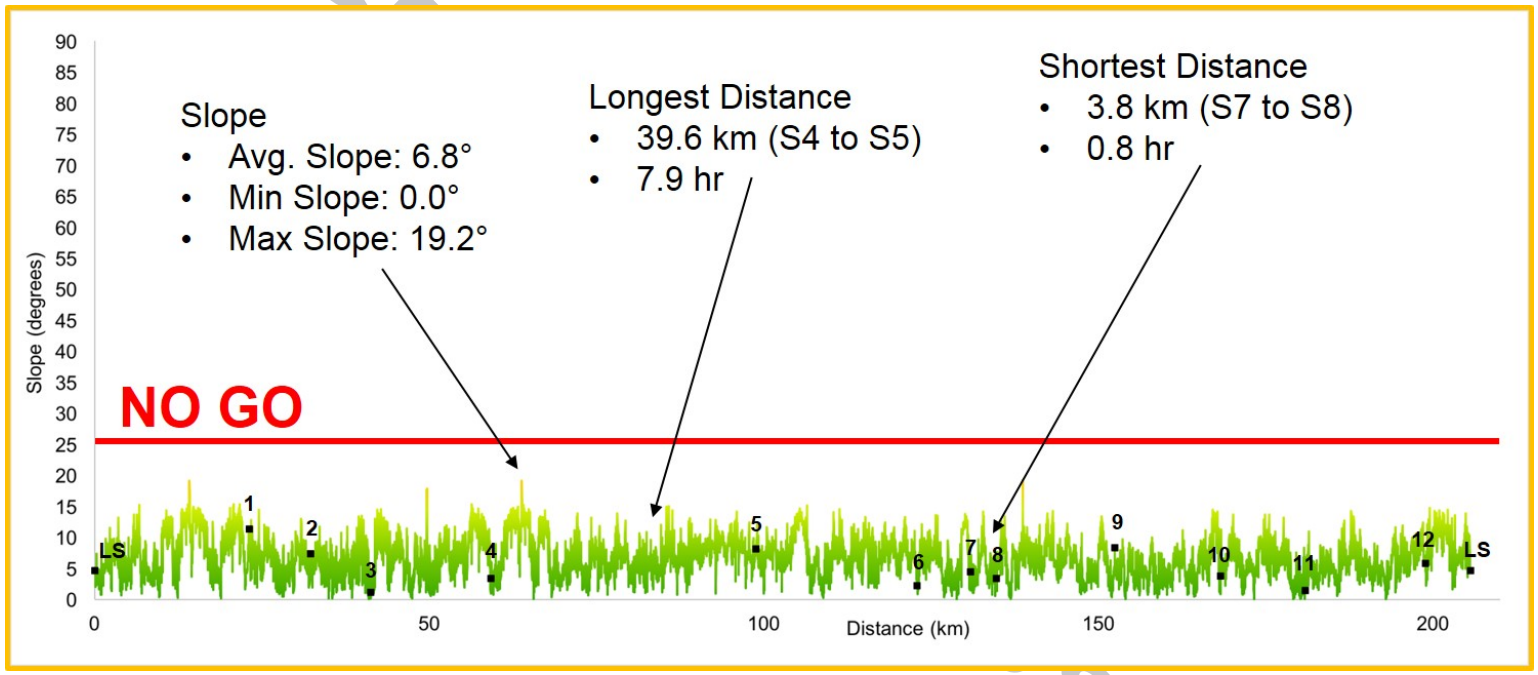

Figure 14: Slope profile for Traverse Loop 1 of Malapert massif. The point of highest slope ('choke point') is found en route to the summit of Malapert ridge, seen in this slope profile just before Station 1 is reached, and again returning along the ridge after passing Station 4. Given higher resolution LROC NAC DEMs it may be possible to maneuver around this point.

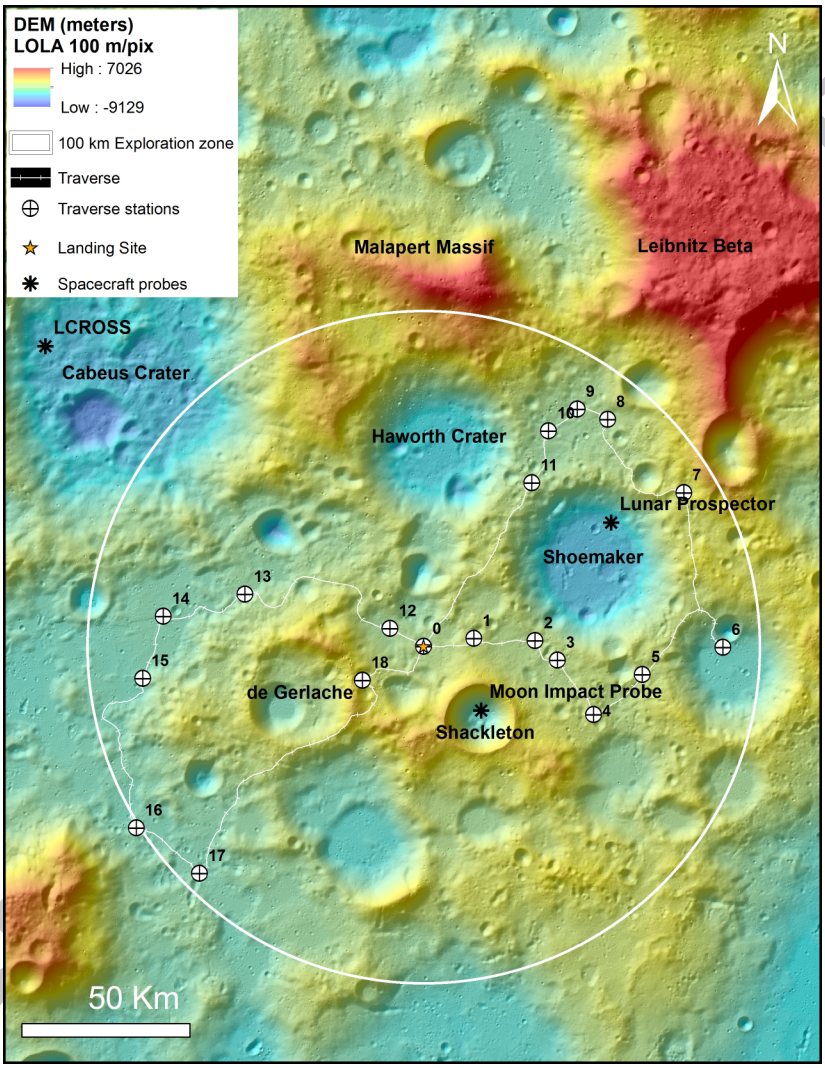

Figure 15: Colorized DEM of the South Pole region displayed on a LROC WAC mosaic of 100 m/pix. Includes traverses, sampling stations, spacecraft probes, and 100 km Mars-forward exploration zone for reference.

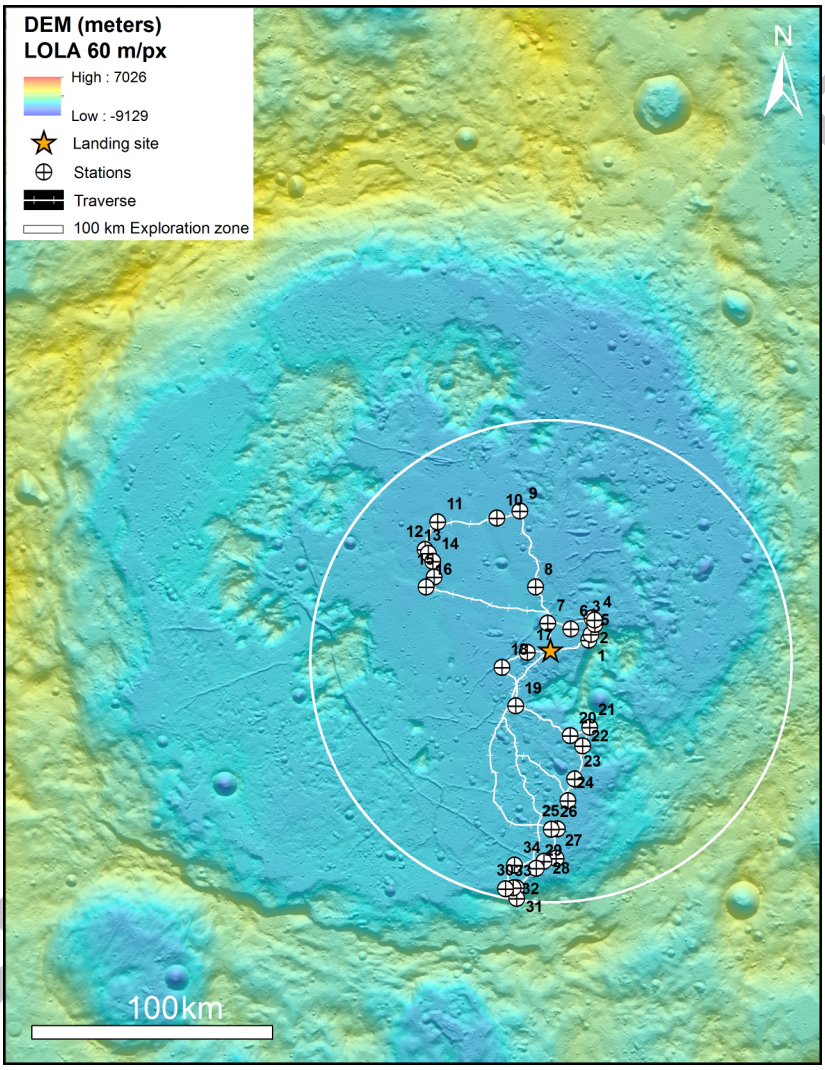

Figure 16: Colorized DEM of Schrödinger basin displayed on a LROC WAC mosaic of 100 m/pix. Includes traverses, sampling stations, and 100 km Mars-forward exploration zone for reference.

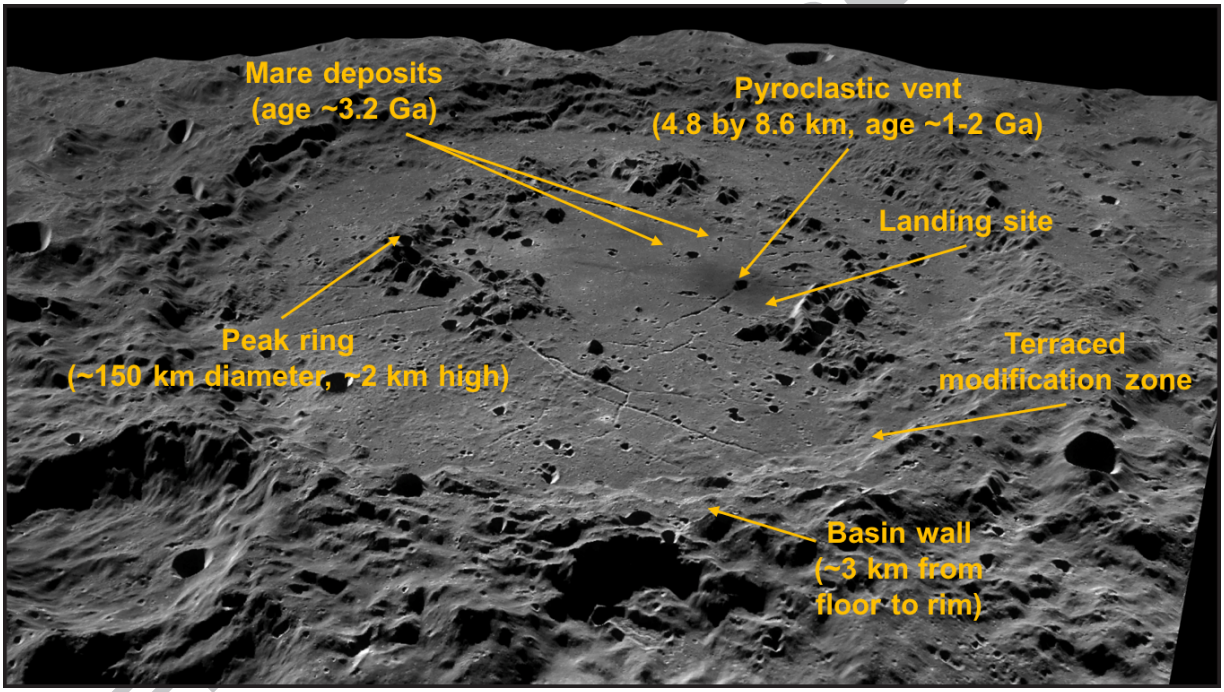

Figure 17: Oblique view of Schrödinger basin exploration zone from 100 m/pix LROC WAC mosaic. Units of interest are labeled.

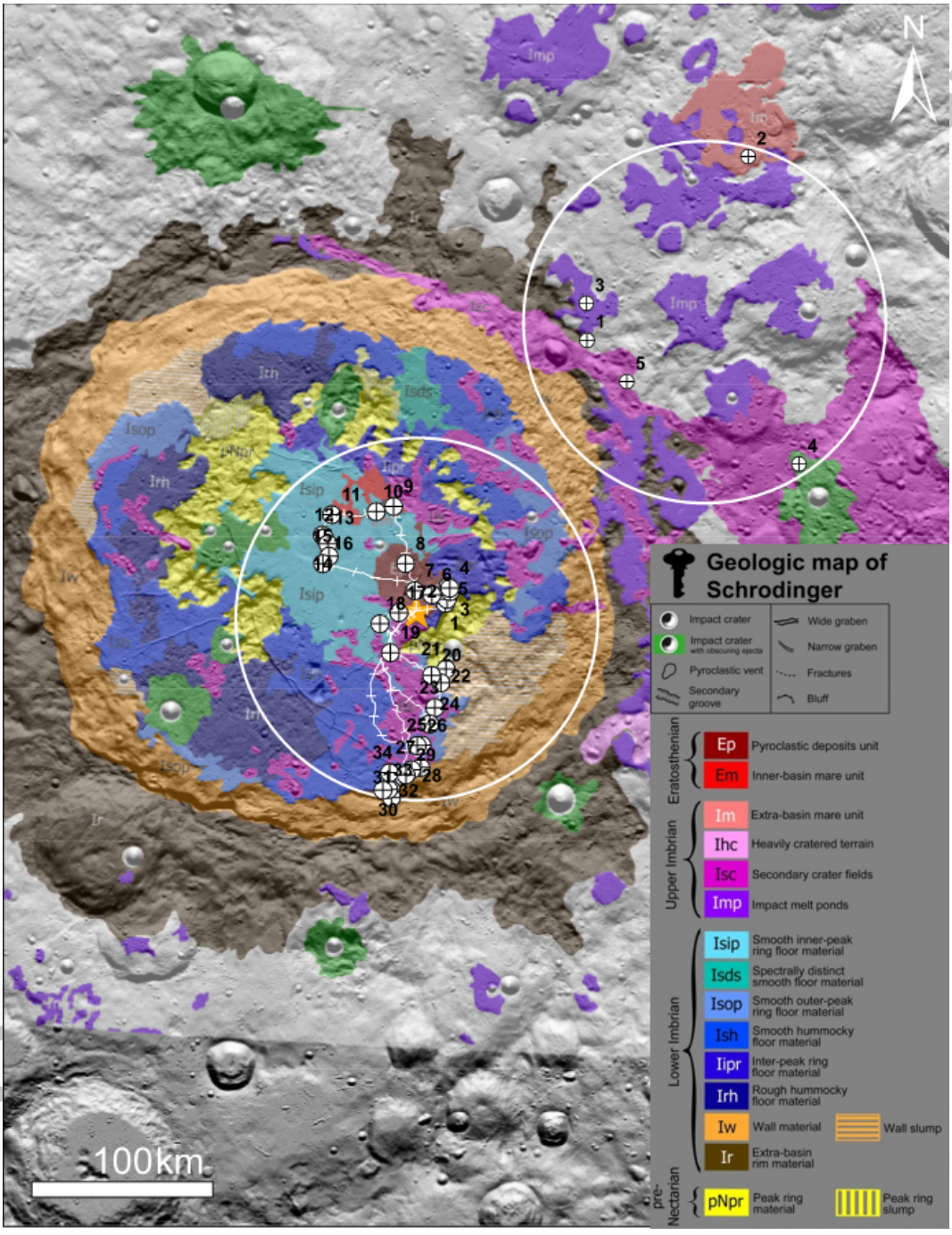

Figure 18: Proposed internal and external landing sites and exploration zones for Schrödinger basin. LOLA 100 m/pixel hillshade overlain with geological map from Kramer et al. (2013) demonstrates the loss of geological variety and novelty if the interior of the basin cannot be accessed by the LERs.

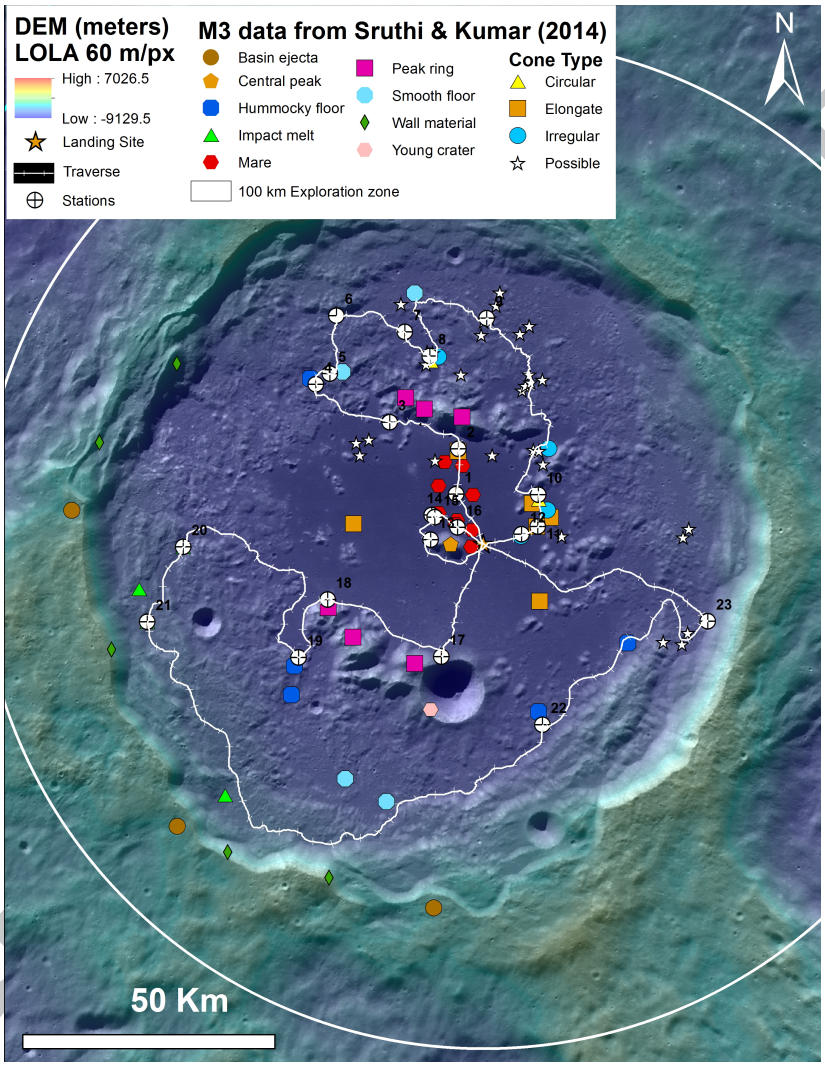

Figure 19: Colorized DEM of Antoniadi crater displayed on a LROC WAC mosaic of 100 m/pix. Includes traverses, sampling stations, and 100 km Mars-forward for reference. Data from Sruthi and Kumar (2014) regarding the locations of their volcanic cones is also included.

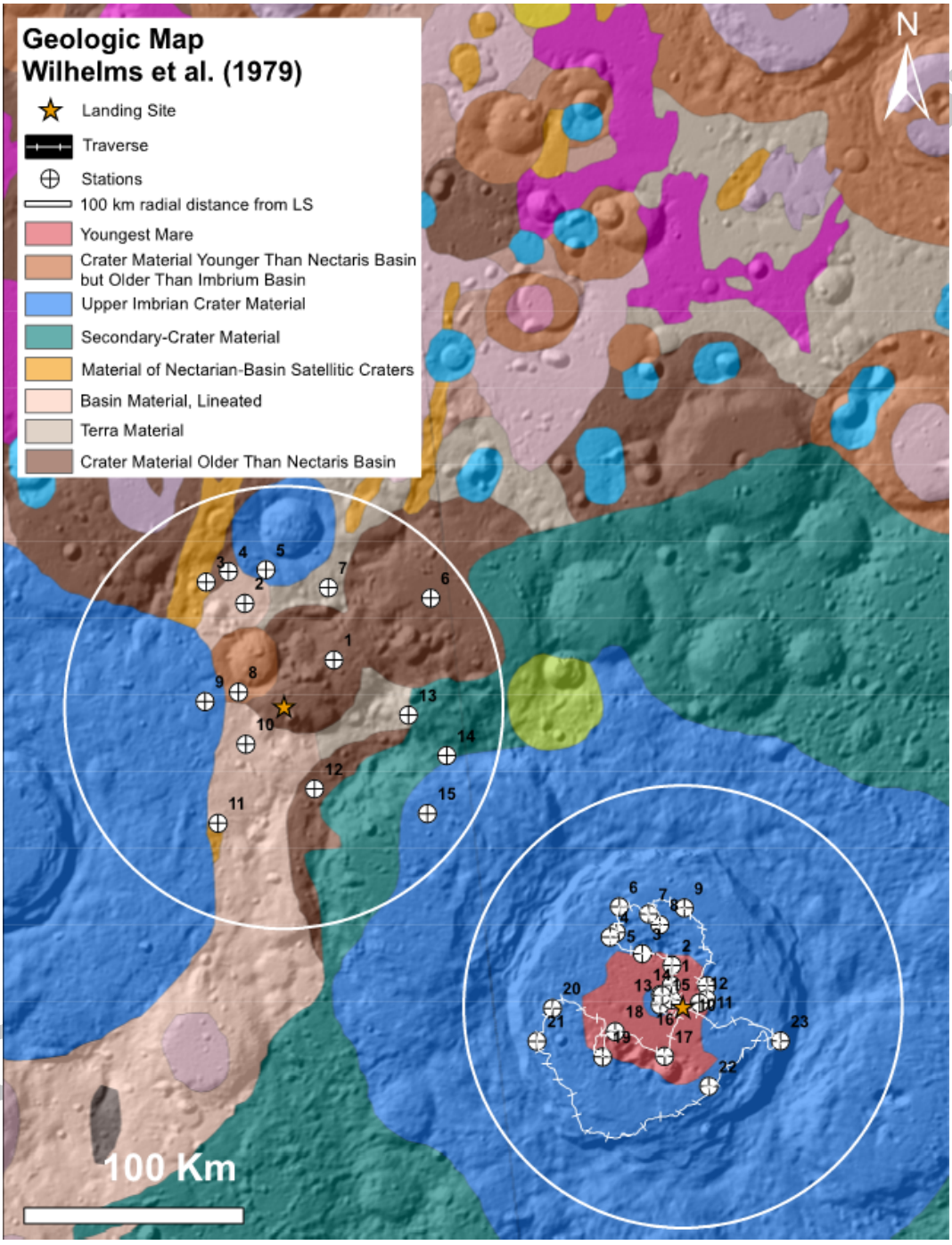

Figure 20: Proposed external (left zone) and internal (right zone) landing sites and exploration zones for Antoniadi crater. LOLA 100 m/pixel hillshade overlain with geological map from Wilhelms et al. (1979) demonstrates the loss of geological novelty if the interior of the crater cannot be accessed by the LER.

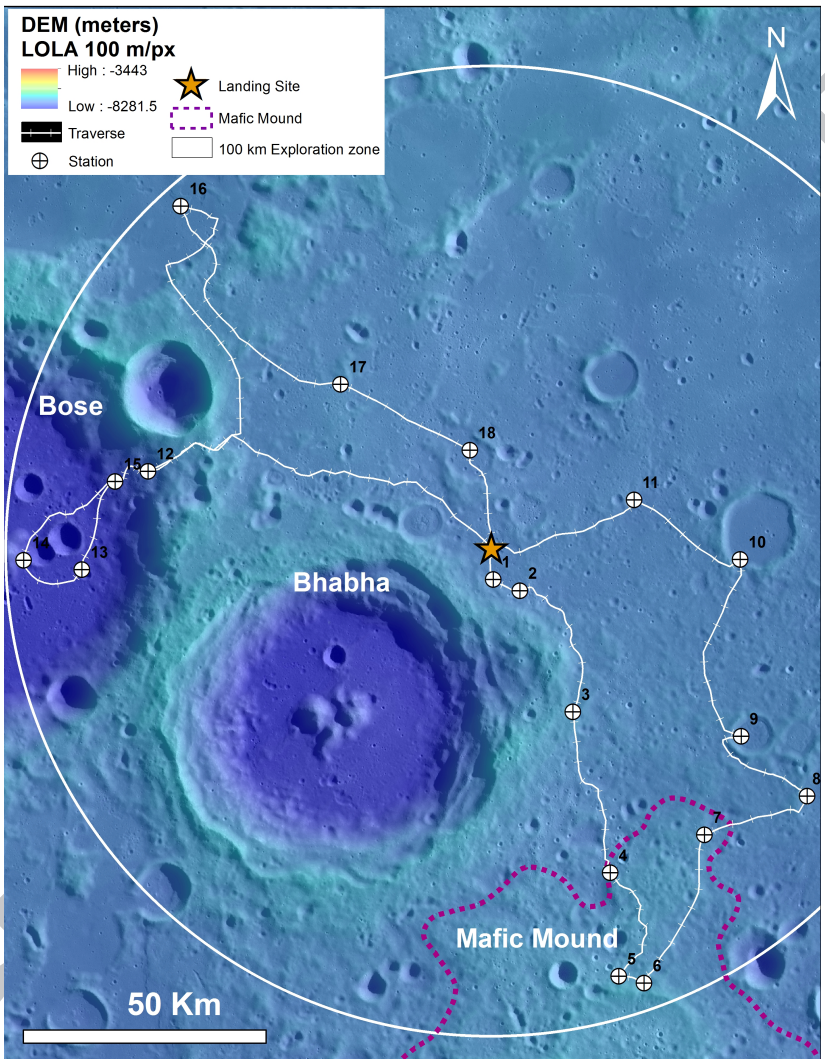

Figure 21: Colorized DEM of SPA basin center containing proposed landing site overlaid on LROC WAC mosaic of 100 m/pix. Includes traverses, sampling stations, and 100 km Mars-forward exploration zone for reference.

Barber, S., Smith, P., Wright, I., Abernathy, F., Anand, M., 2017. ProSPA: the science laboratory for the processing and analysis of lunar polar volatiles within PROSPECT. In: Lunar and Planetary Science Conference. Abstract 2171.

Borst, A. M., Foing, B. H., Davies, G. R., Van Westrenen, W., 2012. Surface mineralogy and stratigraphy of the lunar South Pole-Aitken basin determined from Clementine UV/VIS and NIR data. Planetary and Space Science 68 (1), 76–85.

Bunte, M. K., Porter, S., Robinson, M. S., 2011. A sortie mission to Schrödinger basin as reconnaissance for future exploration. Geological Society of America Special Papers 483, 533–546.

Burns, J. O., Kring, D. A., Hopkins, J. B., Norris, S., Lazio, T. J. W., Kasper, J., 2013. A lunar L2-farside exploration and science mission concept with the Orion multi-purpose crew vehicle and a teleoperated lander/rover. Advances in Space Research 52 (2), 306 – 320.

Bussey, D., McGovern, J., Spudis, P., Neish, C., Noda, H., Ishihara, Y., Sørensen, S. A., 2010. Illumination conditions of the south pole of the Moon derived using Kaguya topography. Icarus 208 (2), 558–564.

Carpenter, J., Barber, S., Cerroni, P., Fisackerly, R., Fumagalli, A., Houdou, B., Howe, C., Magnani, P., Morse, A., Monchieri, E., Reiss, P., Richter, L., Rizzi, F., Sheridan, S., Waugh, L., Wright, I., 2014. Accessing and assessing lunar resources with PROSPECT. In: Annual Meeting of the Lunar Exploration Analysis Group. Abstract 3018.

Chin, G., Brylow, S., Foote, M., Garvin, J., Kasper, J., Keller, J., Litvak, M., Mitrofanov, I., Paige, D., Raney, K., Robinson, M., Sanin, A., Smith, D., Spence, H., Spudis, P., Stern, S. A., Zuber, M., Apr 2007. Lunar Reconnaissance Orbiter overview: the instrument suite and mission. Space Science Reviews 129 (4), 391–419.

Cintala, M. J., Grieve, R. A., 1998. Scaling impact melting and crater dimensions: Implications for the lunar cratering record. Meteoritics & Planetary Science 33 (4), 889–912.

Clark, P. E., Bleacher, J., Mest, S., Petro, N., Leshin, L., 2009. Lunar field exploration scenarios for a south pole outpost. In: Lunar and Planetary Science Conference XXXX Abstract 1135.

Cohen, B. A., Swindle, T. D., Kring, D. A., 2000. Support for the lunar cataclysm hypothesis from lunar meteorite impact melt ages. Science 290, 1754–1756.

Colaprete, A., Schultz, P., Heldmann, J., Wooden, D., Shirley, M., Ennico, K., Hermalyn, B., Marshall, W., Ricco, A., Elphic, R. C., Goldstein, D., 2010. Detection of water in the LCROSS ejecta plume. Science 330 (6003), 463–468.

Connolly, J. F., 2006. Constellation program overview. NASA Presentation.

Costes, N., Farmer, J., George, E., 1972. Mobility performance of the Lunar Roving Vehicle: terrestrial studies - Apollo 15 results. Tech. Rep. TR R-401, National Aeronautics and Space Administration.

De Rosa, D., Bussey, B., Cahill, J. T., Lutz, T., Crawford, I. A., Hackwill, T., van Gasselt, S., Neukum, G., Witte, L., McGovern, A., Grindrod, P. M., Carpenter, J. D., 2012. Characterisation of potential landing sites for the European Space Agency's Lunar Lander project. Planetary and Space Science 74 (1), 224 – 246, scientific Preparations For Lunar Exploration.

Dominov, E., Mest, S. C., 2009. Geology of Antoniadi crater, South Pole-Aitken basin. In: Lunar and Planetary Science Conference XXXX, Abstract 1460.

Elphic, R., Eke, V., Teodoro, L., Lawrence, D., Bussey, D., 2007. Models of the distribution and abundance of hydrogen at the lunar south pole. Geophysical Research Letters 34 (13).

Eppler, D., Adams, B., Archer, D., Baiden, G., Brown, A., Carey, W., Cohen, B., Condit, C., Evans, C., Fortezzo, C., Garry, B., Graff, T., Gruener, J., Heldmann, J., Hodges, K., HÃűrz, F., Hurtado, J., Hynek, B., Isaacson, P., Juranek, C., Klaus, K., Kring, D., Lanza, N., Lederer, S., Lofgren, G., Marinova, M., May, L., Meyer, J., Ming, D., Monteleone, B., Morisset, C., Noble, S., Rampe, E., Ricec, J., Schutt, J., Skinner, J., Tewksbury-Christile, C. M., Tewksbury, B. J., Vaughan, A., Yingst, A., Young, K.,

2013. Desert Research and Technology Studies (DRATS) 2010 science operations: operational approaches and lessons learned for managing science during human planetary surface missions. Acta Astronautica 90 (2), 224–241.

Fagan, A. L., Ennis, M. E., Pogue, J. N., Porter, S., Snape, J. F., Neal, C. R., Kring, D. A., 2010. Science-rich mission sites within South Pole-Aitken basin. In: Lunar and Planetary Science Conference XXXXI Abstract 2467.

Gaddis, L. R., Staid, M. I., Tyburczy, J. A., Hawke, B. R., Petro, N. E., 2003. Compositional analyses of lunar pyroclastic deposits. Icarus 161 (2), 262–280.

Gibson, K. E., Jolliff, B. L., 2011. Correlation of surface units and FeO concentrations in the South Pole-Aitken basin interior. In: Lunar and Planetary Science Conference XXXXII Abstract 2326.

Green, R. O., Pieters, C., Mouroulis, P., Eastwood, M., Boardman, J., Glavich, T., Isaacson, P., Annadurai, M., Besse, S., Barr, D., Buratti, B., Cate, D., Chatterjee, A., Clark, R., Cheek, L., Combe, J., Dhingra, D., Essandoh, V., Geier, S., Goswami, J. N., Green, R., Haemmerle, V., Head, J., Hovland, L., Hyman, S., Klima, R., Koch, T., Kramer, G., Kumar, A. S. K., Lee, K., Lundeen, S., Malaret, E., McCord, T., McLaughlin, S., Mustard, J., Nettles, J., Petro, N., Plourde, K., Racho, C., Rodriquez, J., Runyon, C., Sellar, G., Smith, C., Sobel, H., Staid, M., Sunshine, J., Taylor, L., Thaisen, K., Tompkins, S., Tseng, H., Vane, G., Varanasi, P., White, M., Wilson, D., 2011. The Moon Mineralogy Mapper (M3) imaging spectrometer for lunar science: instrument description, calibration, on-orbit measurements, science data calibration and on-orbit validation. Journal of Geophysical Research: Planets 116 (E10).

Harland, D., 2008. Exploring the Moon: the Apollo expeditions, 2nd Edition. Praxis Publishing Ltd, Chichester, UK.

Harrison, D. A., Ambrose, R., Bluethmann, B., Junkin, L., 2008. Next generation rover for lunar exploration. In: Aerospace Conference. pp. 1–14.

Haruyama, J., Ohtake, M., Matsunaga, T., Morota, T., Honda, C., Yokota, Y., Abe, M., Ogawa, Y., Miyamoto, H., Iwasaki, A., Pieters, C. M., Asada, N., Demura, H., Hirata, N., Terazono, J., Sasaki, S., Saiki, K., Yamaji, A.,

Torii, M., L., J. J., 2009. Long-lived volcanism on the lunar farside revealed by SELENE terrain camera. Science 323 (5916), 905–908.

Haruyama, J., Ohtake, M., Matsunaga, T., Morota, T., Honda, C., Yokota, Y., Pieters, C. M., Hara, S., Hioki, K., Saiki, K., Miyamoto, H., Iwasaki, A., Abe, M., Ogawa, Y., Takeda, H., Shirao, M., Yamaji, A., Josset, J. L., 2008. Lack of exposed ice inside lunar south pole Shackleton crater. Science 322 (5903), 938–939.

Head, J. W., Fassett, C. I., Kadish, S. J., Smith, D. E., Zuber, M. T., Neumann, G. A., Mazarico, E., 2010. Global distribution of large lunar craters: implications for resurfacing and impactor populations. Science 329, 1504–1507.

Hiesinger, H., Head, J. W., Wolf, U., Jaumann, R., Neukum, G., 2002. Lunar mare basalt flow units: Thicknesses determined from crater size-frequency distributions. Journal of Geophysical Research Letters 29 (8).

Hiesinger, H., Head, J. W., Wolf, U., Jaumann, R., Neukum, G., 2003. Ages and stratigraphy of mare basalts in Oceanus Procellarum, Mare Nubium, Mare Cognitum, and Mare Insularum. Journal of Geophysical Research 108 (E7).

Hiesinger, H., van der Bogert, C, H., Pasckert, J.-H., Schmedemann, N., Robinson, M., Jolliff, B., Petro, N., 2012. New crater size-frequency distribution measurements of the South Pole Aitken basin. In: Lunar and Planetary Science Conference 43. p. Abstract 2863.

Hopkins, J., Pratt, C., Hall, S., Scott, A., Farquar, R., Dunham, D., 2013. Proposed orbits and trajectories for human missions to the Earth-Moon L2 region. In: 64th International Astronautical Congress. Beijing.

Huang, J., Xiao, Z., Flahaut, J., Martinot, M., Head, J., Xiao, X., Xie, M., Xiao, L., 2018. Geological characteristics of Von Kármán crater, northwestern South Pole-Aitken Basin: Chang'E-4 landing site region. Journal of Geophysical Research: Planets.

Hufenbach, B., Laurini, K. C., Satoh, N., Lange, C., Martinez, R., Hill, J., Landgraf, M., Bergamasco, A., 2015. International missions to lunar vicinity and surface-near- term mission scenario of the global space exploration roadmap. In: 66th International Astronomical Congress.

Hurwitz, D. M., Kring, D. A., 2013. Composition and structure of the South Pole-Aitken basin impact melt sheet. In: Lunar and Planetary Science Conference XXXXI, Abstract 2224.

Hurwitz, D. M., Kring, D. A., 2014. Differentiation of the South Pole-Aitken basin impact melt sheet: implications for lunar exploration. Journal of Geophysical Research (Planets) 119, 1110–1133.

Hurwitz, D. M., Kring, D. A., 2015. Potential sample sites for South Pole-aitken basin impact melt within the Schrödinger basin. Earth and Planetary Science Letters 427, 31–36.

International Space Exploration Coordination Group, 2013. The global exploration roadmap. National Aeronautics and Space Administration.

International Space Exploration Coordination Group, 2018. The global exploration roadmap. National Aeronautics and Space Administration.

Ivanov, M., Hiesinger, H., Orgel, C., Pasckert, J., van der Bogert, C., Head, J., In Press. Geologic history of the northern portion of the South Pole-Aitken basin on the Moon. Journal of Geophysical Research.

Jaumann, R., Hiesinger, H., Anand, M., Crawford, I., Wagner, R., Sohl, F., Jolliff, B., Scholten, F., Knapmeyer, M., Hoffmann, H., Hussmann, H., Grott, M., Hempel, S., Köhler, U., Krohn, K., Schmitz, N., Carpenter, J., Wieczorek, M., Spohn, T., Robinson, M., Oberst, J., 2012. Geology, geochemistry, and geophysics of the Moon: status of current understanding. Planetary and Space Science 74 (1), 15–41.

Jolliff, B. L., Alkalai, L., Pieters, C. M., Head, J. W., Papanastassiou, D. A., Bierhaus, E. B., 2010. Sampling the South Pole-Aitken basin: Objectives and site selection criteria. In: Lunar and Planetary Science Conference 41. Abstract 2450.

Jolliff, B. L., Gillis, J. J., Haskin, L. A., Korotev, R. L., Wieczorek, M. A., 2000. Major lunar crustal terranes: surface expressions crust-mantle origins. Journal of Geophysical Research 105 (E2), 4197–4216.

Jolliff, B. L., Haskin, L. A., Korotev, R. L., Papike, J. J., Shearer, C. K., Pieters, C. M., Cohen, B., 2003. Scientific expectations from a sample

of regolith and rock fragments from the interior of the lunar South Pole-Aitken basin. In: Lunar and Planetary Science Conference 34. Abstract 1989.

Jolliff, B. L., Shearer, C. K., Papanastassiou, D. A., Liu, Y., 2017. Why do we need samples from the Moon's South Pole-Aitken basin and what would we do with them? In: Lunar and Planetary Science Conference 48. Abstract 1300.

Korotev, R., 2000. The great lunar hot spot and the composition and origin of the Apollo mafic ("LKFM") impact-melt breccias. Journal of Geophysical Research 105 (E2), 4307–4345.

Kramer, G. Y., Kring, D. A., Nahm, A. L., Pieters, C. M., 2013. Spectral and photogeologic mapping of Schrödinger basin and implications for post-South Pole-Aitken impact deep subsurface stratigraphy. Icarus 233, 131–148.

Kring, D., 2007. Lunar Exploration Initiative: lunar EVA sample mass.

Kring, D., 2017. The lunar electric rover (aka space exploration vehicle) as a geological tool. In: Fifth European Lunar Symposium. p. 125.

Kring, D., Bleacher, J., Garry, W., Love, S., Young, K., 2017. The utility of a small pressurized rover with suit ports for lunar exploration: a geologist's perspective. In: NASA Exploration Science Forum.

Kring, D. A., 2011. Lunar surface systems study: Malapert massif, unpublished manuscript.

Kring, D. A., 2014. Exploring the Schrödinger and South Pole-Aitken basins on the lunar farside. In: 40th COSPAR Scientific Assembly. Vol. 40.

Kring, D. A., Durda, D. D., 2012. A global lunar landing site study to provide the scientific context for exploration of the Moon. Lunar and Planetary Institute, contribution 1694.

Kring, D. A., Kramer, G. Y., Bussey, D. B. J., Hurley, D. M., 2014. Prominent volcanic source of volatiles in the south polar region of the Moon. In: Annual Meeting of the Lunar Exploration Analysis Group. Vol. 1820.

Kring, D. A., Kramer, G. Y., Collins, G. S., Potter, R. W. K., Chandnani, M., Oct. 2016. Peak-ring structure and kinematics from a multi-disciplinary study of the Schrödinger impact basin. Nature Communications 7, 13161.

Kring, D. A., Kramer, G. Y., Potter, R. W. K., 2013. Interpreting the depth of origin of the Schrödinger peak ring and implications for other impact basins. In: Large Meteorite Impacts and Planetary Evolution V. LPI Contributions 1737, p. 3069.

Landgraf, M., Carpenter, J., Sawada, H., 2015. HERACLES concept - an international lunar exploration architecture study. In: Lunar Exploration Analysis Group.

Lawrence, D., Elphic, R., Feldman, W., Prettyman, T., Gasnault, O., Maurice, S., 2003. Small-area thorium features on the lunar surface. Journal of Geophysical Research 108 (E9).

Lawrence, D., Puetter, R., Elphic, R., Feldman, W., Hagerty, J., Prettyman, T., Spudis, P., 2007. Global spatial deconvolution of Lunar Prospector Th abundances. Geophysical Research Letters 34 (L03201).

Lawrence, D. J., Feldman, W. C., Barraclough, B. L., Binder, A. B., Elphic, R. C., Maurice, S., Thomsen, D. R., 1998. Global elemental maps of the Moon: The Lunar Prospector gamma-ray spectrometer. Science 281 (5382), 1484–1489.

Lawrence, D. J., Feldman, W. C., Elphic, R. C., Little, R. C., Prettyman, T. H., Maurice, S., Lucey, P. G., Binder, A. B., 2002. Iron abundances on the lunar surface as measured by the Lunar Prospector gamma-ray and neutron spectrometers. Journal of Geophysical Research: Planets 107 (E12), 1–26.

Lemelin, M., Blair, D., Roberts, C., Runyon, K., Nowka, D., Kring, D., 2014. High-priority lunar landing sites for in situ and sample return studies of polar volatiles. Planetary and Space Science 101, 149–161.

Lockheed Martin, July 2016. Orbital coverage for the South Pole-Aitken basin center.

Lucey, P. G., Taylor, G. J., Hawke, B. R., Spudis, P. D., 1998. Feo and TiO concentrations in the South Pole-Aitken basin: Implications for mantle

composition and basin formation. Journal of Geophysical Research 103, 3701–3708.

Lunar Exploration Science Working Group, 1995. Lunar surface exploration strategy - final report. Tech. rep.

Mahaffy, P. R., Webster, C. R., Cabane, M., Conrad, P. G., Coll, P., Atreya, S. K., Arvey, R., Barciniak, M., Benna, M., Bleacher, L., Brinckerhoff, W. B., Eigenbrode, J. L., Carignan, D., Cascia, M., Chalmers, R. A., Dworkin, J. P., Errigo, T., Everson, P., Franz, H., Farley, R., Feng, S., Frazier, G., Freissinet, C., Glavin, D. P., Harpold, D. N., Hawk, D., Holmes, V., Johnson, C. S., Jones, A., Jordan, P., Kellogg, J., Lewis, J., Lyness, E., Malespin, C. A., Martin, D. K., Maurer, J., McAdam, A. C., McLennan, D., Nolan, T. J., Noriega, M., Pavlov, A. A., Prats, B., Raaen, E., Sheinman, O., Sheppard, D., Smith, J., Stern, J. C., Tan, F., Trainer, M., Ming, D. W., Morris, R. V., Jones, J., Gundersen, C., Steele, A., Wray, J., Botta, O., Leshin, L. A., Owen, T., Battel, S., Jakosky, B. M., Manning, H., Squyres, S., Navarro-González, R., McKay, C. P., Raulin, F., Sternberg, R., Buch, A., Sorensen, P., Kline-Schoder, R., Coscia, D., Szopa, C., Teinturier, S., Baffes, C., Feldman, J., Flesch, G., Forouhar, S., Garcia, R., Keymeulen, D., Woodward, S., Block, B. P., Arnett, K., Miller, R., Edmonson, C., Gorevan, S., Mumm, E., Sep 2012. The Sample Analysis at Mars investigation and instrument suite. Space Science Reviews 170 (1), 401–478.

Mandt, K. E., Greathouse, T. K., Retherford, K. D., Gladstone, G. R., Jordan, A. P., Lemelin, M., Koeber, S. D., Bowman-Cisneros, E., Patterson, G. W., Robinson, M., Lucey, P. G., Hendrix, A. R., Hurley, D., Stickle, A. M., Pryor, W., 2016. Lro-lamp detection of geologically young craters within lunar permanently shaded regions. Icarus 273, 114–120.

Massachusetts Institute of Technology, 2016. Percentage Earth visibility map. online.
URL `http://imbrium.mit.edu/EXTRAS/ILLUMINATION/RELEASE_2014/IMG`

Mazanek, D. D., Troutman, P. A., Culbert, C. J., Leonard, M. J., Spexarth, G. R., 2009. Surface buildup scenarios and outpost architectures for Lunar Exploration. In: 2009 IEEE Aerospace conference. pp. 1–23.

Mazarico, E., Neumann, G., Smith, D., Zuber, M., Torrence, M., 2011. Illumination conditions of the lunar polar regions using LOLA topography. Icarus 211 (2), 1066 – 1081.

Moratto, Z. M., Broxton, M. J., Beyer, R. A., Lundy, M., Husmann, K., Mar. 2010. Ames Stereo Pipeline, NASA's open source automated stereogrammetry software. In: Lunar and Planetary Science Conference. Vol. 41 of Lunar and Planetary Science Conference. p. 2364.

Morbidelli, A., Marchi, S., Bottke, W. F., Kring, D. A., 2012. A sawtooth-like timeline for the first billion years of lunar bombardment. Earth and Planetary Science Letters 355, 144–151.

Moriarty, D. P., Pieters, C. M., 2015. The nature and origin of Mafic Mound in the South Pole-aitken Basin. Geophysical Research Letters 42 (19), 7907–7915.

Moriarty, D. P., Pieters, C. M., 2016. Impact melt and magmatic processes in central South Pole-Aitken basin. In: Lunar and Planetary Science Conference 47. Abstract 1735.

Moriarty, D. P., Pieters, C. M., 2018. The character of South Pole-Aitken basin: patterns of surface and sub-surface composition. Journal of Geophysical Research: Planets 123.

Nakamura, R., Matsunaga, T., Ogawa, Y., Yamamoto, S., Hiroi, T., Saiki, K., Hirata, N., Arai, T., Kitazato, K., Takeda, H., Sugihara, T., Kodama, S., Ohtake, M., Haruyama, J., Yokota, Y., 2009. Ultramafic impact melt sheet beneath the South Pole-Aitken basin on the Moon. Geophysical Research Letters 36 (22).

National Research Council, 2007. The scientific context for exploration of the Moon: final report. Washington, DC: The National Academies Press.

Oberbeck, V. R., Quaide, W. L., 1968. Genetic implications of Lunar regolith thickness variations. Icarus 9 (1), 446 – 465.

Öhman, T., Kring, D. A., 2012. Photogeologic analysis of impact melt-rich lithologies in Kepler crater that could be sampled by future missions. Journal of Geophysical Research (Planets) 117 (E12).

Ohtake, M., Uemoto, K., Yokota, Y., Morota, T., Yamamoto, S., Nakamura, R., Haruyama, J., Iwata, T., Matsunaga, T., Ishihara, I., 2014. Geologic structure generated by large-impact basin formation observed at the South Pole-Aitken basin on the Moon. Geophysical Research Letters 41, 2738–2745.

Orgel, C., Michael, G., Fassett, C. I., van der Bogert, C. H., Riedel, C., Kneissl, T., Hiesinger, H., 2018. Ancient bombardment of the inner solar system: reinvestigation of the fingerprints of different impactor populations on the lunar surface. Journal of Geophysical Research: Planets 123.

O'Sullivan, K., Kohout, T., Thaisen, K., Kring, D., 2011. Calibrating several key lunar stratigraphic units representing 4 b.y. of lunar history within Schrödinger basin. Recent Advances and Current Research Issues in Lunar Stratigraphy. Geological Society of America Special Papers 477, 117–127.

Paige, D. A., Siegler, M. A., Zhang, J. A., Hayne, P. O., Foote, E. J., Bennett, K. A., Vasavada, A. R., Greenhagen, B. T., Schofield, J. T., McCleese, D. J., Foote, M. C., DeJong, E., Bills, B. G., Hartford, W., Murray, B. C., Allen, C. C., Snook, K., Soderblom, L. A., Calcutt, S., Taylor, F. W., Bowles, N. E., Bandfield, J. L., Elphic, R., Ghent, R., Glotch, T. D., Wyatt, M. B., Lucey, P. G., 2010. Diviner lunar radiometer observations of cold traps in the Moon's south polar region. Science 330 (6003), 479–482.

Pasckert, J. H., Hiesinger, H., van der Bogert, C. H., 2018. Lunar farside volcanism in and around the South Pole-Aitken basin. Icarus 299, 538 – 562.

Petro, N. E., Jolliff, B. L., 2011. Basin and crater ejecta contributions to the South Pole-Aitken basin (SPA) regolith; positive implications for robotic surface samples. Journal of Geophysical Research (Planets) 109 (E6).

Petro, N. E., Pieters, C. M., 2004. Surviving the heavy bombardment: ancient material at the surface of South Pole-Aitken basin. Journal of Geophysical Research (Planets) 109 (E6).

Pieters, C. M., Head, J. W., Gaddis, L., Jolliff, B., Duke, M., 2001. Rock types of South Pole-Aitken basin and extent of basaltic volcanism. Journal of Geophysical Research (Planets) 106 (E11), 28001–28022.

Potts, N. J., Gullikson, A. L., Curran, N. M., Dhaliwal, J. K., Leader, M. K., Rege, R. N., Kring, D. A., 2015. Robotic traverse and sample return strategies for a lunar farside mission to the Schrödinger basin. Advances in Space Research 55 (4), 1241–1254.

Runyon, K., Blair, D. M., Lemelin, M., Nowka, D., Roberts, C. E., Paige, D. A., Spudis, P., Kring, D., 2012. Volatiles at the lunar south pole: a case study for a mission to Amundsen. In: Lunar and Planetary Science XLIII Abstract 1619.

Sanin, A. B., Mitrofanov, I. G., Litvak, M. L., Malakhov, A., Boynton, W. V., Chin, G., Droege, G., Evans, L. G., Garvin, J., Golovin, D. V., Harshman, K., McClanahan, T. P., Mokrousov, M. I., Mazarico, E., Milikh, G., Neumann, G., Sagdeev, R., Smith, D. E., Starr, R. D., Zuber, M. T., 2012. Testing lunar permanently shadowed regions for water ice: LEND results from LRO. Journal of Geophysical Research: Planets 117 (E12).

Senthil Kumar, P., Keerthi, V., Senthil Kumar, A., Mustard, J., Gopala Krishna, B., Amitabh, Ostrach, L. R., Kring, D. A., Kiran Kumar, A. S., Goswami, J. N., 2013. Gullies and landslides on the moon: evidence for dry-granular flows. Journal of Geophysical Research: Planets 118 (2), 206–223.

Senthil Kumar, P., Sruthi, U., Krishna, N., Lakshmi, K. J. P., Menon, R., Amitabh, Gopala Krishna, B., Kring, D. A., Head, J. W., Goswami, J. N., Kiran Kumar, A. S., 2016. Recent shallow moonquake and impact-triggered boulder falls on the Moon: new insights from the Schrödinger basin. Journal of Geophysical Research: Planets 121 (2), 147–179, 2015JE004850.

Shearer, C., Neal, C., Borg, L., Jolliff, B., Papanastassiou, D., Treiman, A., Floss, C., Rutherford, M., Norman, M., Farquhar, J., May 2007. Analysis of lunar sample mass capability for the lunar exploration architecture.

Shoemaker, E., Robinson, M., Eliason, E., 1994. The south pole region of the Moon as seen by Clementine. Science 266 (5192), 1851–1854.

Smith, D. E., Zuber, M. T., Neumann, G. A., Lemoine, F. G., Mazarico, E., Torrence, M. H., McGarry, J. F., Rowlands, D. D., Head, J. W., Duxbury, T. H., Aharonson, O., Lucey, P. G., Robinson, M. S., Barnouin, O. S.,

Cavanaugh, J. F., Sun, X., Liiva, P., Mao, D., Smith, J. C., Bartels, A. E., 2010. Initial observations from the Lunar Orbiter Laser Altimeter (LOLA). Geophysical Research Letters 37 (18).

Spudis, P. D., Bussey, B., Plescia, J., Josset, J. L., Beau-vivre, S., 2008. Geology of Shackleton crater and the South Pole of the Moon. Geophysical Research Letters 35 (14).

Sruthi, U., Kumar, P. S., 2014. Volcanism on farside of the Moon: New evidence from Antoniadi in South Pole-Aitken basin. Icarus 242, 249–268.

Steenstra, E. S., Martin, D. J., McDonald, F. E., Paisarnsombat, S., Venturino, C., O'Hara, S., Calzada-Diaz, A., Bottoms, S., Leader, M. K., Klaus, K. K., van Westrenen, W., 2016. Analyses of robotic traverses and sample sites in the Schrödinger basin for the HERACLES human-assisted sample return mission concept. Advances in Space Research 58 (6), 1050–1065.

Stöffler, D., Ryder, G., 2001. Stratigraphy and isotope ages of lunar geologic units: chronological standard for the inner solar system. Space Sci. Rev. 96, 9–54.

Stuart-Alexander, D., 1978. Geological map of the central far side of the Moon. United States Geological Service Map (I-1047).

Tera, F., Papanastassiou, D. A., Wasserburg, G. J., 1974. Isotopic evidence for a terminal lunar cataclysm. Earth Planet. Sci. Lett. 22, 1–21.

Vago, J. L., Westall, F., Pasteur Instrument Teams, Landing Site Selection Working Group, Other Contributors, Coates, A. J., Jaumann, R., Korablev, O., Ciarletti, V., Mitrofanov, I., Josset, J.-L., De Sanctis, M. C., Bibring, J.-P., Rull, F., Goesmann, F., Steininger, H., Goetz, W., Brinckerhoff, W., Szopa, C., Raulin, F., Westall, F., Edwards, H. G. M., Whyte, L. G., Fairén, A. G., Bibring, J.-P., Bridges, J., Hauber, E., Ori, G. G., Werner, S., Loizeau, D., Kuzmin, R. O., Williams, R. M. E., Flahaut, J., Forget, F., Vago, J. L., Rodionov, D., Korablev, O., Svedhem, H., Sefton-Nash, E., Kminek, G., Lorenzoni, L., Joudrier, L., Mikhailov, V., Zashchirinskiy, A., Alexashkin, S., Calantropio, F., Merlo, A., Poulakis, P., Witasse, O., Bayle, O., Bayón, S., Meierhenrich, U., Carter, J., Garcia-Ruiz, J. M., Baglioni, P., Haldemann, A., Ball, A. J., Debus, A., Lindner, R., Haessig, F., Monteiro, D., Trautner, R., Voland, C., Rebeyre,

P., Goulty, D., Didot, F., Durrant, S., Zekri, E., Koschny, D., Toni, A., Visentin, G., Zwick, M., van Winnendael, M., Azkarate, M., Carreau, C., the ExoMars Project Team, 2017. Habitability on early Mars and the search for biosignatures with the ExoMars Rover. Astrobiology 17 (6-7), 471–510.

Vaughan, W. M., Head, J. W., 2014. Impact melt differentiation in the South Pole-Aitken basin: some observations and speculations. Planetary and Space Science 91, 101–106.

Watson, K., Murray, B. C., Brown, H., 1961. The behavior of volatiles on the lunar surface. Journal of Geophysical Research 66 (9), 3033–3045.

Whitley, R., Landgraf, M., Sato, N., Picard, M., Goodliff, K., Stephenson, K., Narita, S., Gonthier, Y., Cowley, A., Hosseini, S., Schonenborg, R., 06 2017. Global Exploration Roadmap derived concept for human exploration of the Moon. In: Global Space Exploration Conference (GLEX 2017).

Whitley, R., Martinez, R., March 2016. Options for staging orbits in cislunar space. In: 2016 IEEE Aerospace Conference. pp. 1–9.

Wieczorek, M., Phillips, R., 2000. The âĂIJProcellarum KREEP TerraneâĂİ: Implications for mare volcanism and lunar evolution. Journal of Geophysics Research 105 (E8), 20417–20430.

Wieczorek, M. A., Neumann, G. A., Nimmo, F., Kiefer, W. S., Taylor, G. J., Melosh, H. J., Phillips, R. J., Solomon, S. C., Andrews-Hanna, J. C., Asmar, S. W., Konopliv, A. S., Lemoine, F. G., Smith, D. E., Watkins, M. M., Williams, J. G., Zuber, M. T., 2013. The crust of the Moon as seen by GRAIL. Science 339, 671–675.

Wilhelms, D., 1987. The geologic history of the Moon. USGS Special Paper 1348, 302.

Wilhelms, D. E., Howard, K. A., Wilshire, H. G., 1979. Geologic map of the South Pole of the Moon. No. I-1162. Department of the Interior, U. S.

Xiao, L., Zhu, P., Fang, G., Xiao, Z., Zou, Y., Zhao, J., Zhao, N., Yuan, Y., Qiao, L., Zhang, X., Zhang, H., Wang, J., Huang, J., Huang, Q., He, Q., Zhou, B., Ji, Y., Zhang, Q., Shen, S., Li, Y., Gao, Y., 2015. A young

multilayered terrane of the northern Mare Imbrium revealed by Chang'E-3 mission. Science 347 (6227), 1226–1229.

Yamamoto, S., Nakamura, R., Matsunaga, T., Ogawa, Y., Ishihara, Y., Morota, T., Hirata, N., Ohtake, M., Hiroi, T., Yokota, Y., Haruyama, J., 2012. Olivine-rich exposures in the South Pole-Aitken basin. Icarus 218, 331–344.

Zhang, J. A., Paige, D. A., 2009. Cold-trapped organic compounds at the poles of the Moon and Mercury: Implications for origins. Geophysical Research Letters 36 (16).

Zhang, J. A., Paige, D. A., 2010. Correction to "cold-trapped organic compounds at the poles of the Moon and Mercury: implications for origins". Geophysical Research Letters 37 (3).

Zuber, M. T., Smith, D. E., Watkins, M. M., Asmar, S. W., Konopliv, A. S., Lemoine, F. G., Melosh, H. J., Neumann, G. A., Phillips, R. J., Solomon, S. C., Wieczorek, M. A., 2013. Gravity field of the Moon from the Gravity Recovery and Interior Laboratory (GRAIL) mission. Science 339 (6120), 668–671.

List of Figures

Highlights

Tele-operated traverse routes planned between five key SPA landing sites. [73 characters]

Accessibility study reveals potential access into crater interiors. [67 characters]

Multi-duration, crewed exploration of landing sites within the SPA basin maximizes science returns. [99 characters]